Bending boundary layers near the clamped
end of a thin-walled elastic tube

MARTIN C. WALTERS AND ROBERT J. WHITTAKER*

School of Mathematics, University of East Anglia, Norwich Research Park, Norwich, NR4 7TJ, UK
*Corresponding author: http://robert.mathmos.net/

We consider small-amplitude deformations of a long thin-walled elastic tube, caused by a pressure difference between the interior and exterior. The tube initially has a uniform elliptical cross-section and is subject to a large axial pre-stress. The tube length and wall thinness can be exploited to derive simplified models of the wall mechanics. Such models typically neglect effects such as axial bending, which are small over most of the tube but contain higher-order axial derivatives. The resulting models are unable to satisfy the full set of clamped boundary conditions where an elastic section of tube is joined to a rigid support. In this work, we examine the asymptotic boundary layers that arise near the clamped end of an elastic-walled tube, which allow a bulk solution to a simplified model in the interior to be matched to the boundary conditions at the tube ends. We consider the region of parameter space where the width of the thinnest bending boundary-layer is small compared with the tube diameter, but still much larger than the thickness of the tube wall. Within this region, we find three distinct regimes which give rise to different sets of nested boundary layers involving different physical effects. Our matched asymptotic solutions show excellent agreement with an exact solution in a case where the full problem can be solved analytically.

Keywords: Starling resistor; solid mechanics; boundary-layers; elastic-walled tube; tube laws.

1. Introduction

Fluid conveying elastic-walled tubes occur in many different biological, medical, and industrial contexts. Instabilities in such flows, involving fluid-structure interaction between the conveyed fluid and the tube wall, are well-known and have been extensively studied, using experimental, numerical, and asymptotic techniques (see, e.g., the reviews by Heil & Jensen, 2003; Grotberg & Jensen, 2004; Heil & Hazel, 2011).

The canonical experimental setup for studying such flows is know as the 'Starling resistor'. As shown in Figure 1, a finite length of elastic-walled tube is clamped between two rigid tubes and placed inside a pressure chamber. Fluid is driven through the tubes by imposing a pressure difference between the inlet and outlet, or by using a volumetric pump at one end. The external pressure in the chamber can be adjusted to alter the degree of collapse of the elastic section of the tube. The axial tension in the elastic tube can also be adjusted by altering the distance between the two rigid sections of tube after
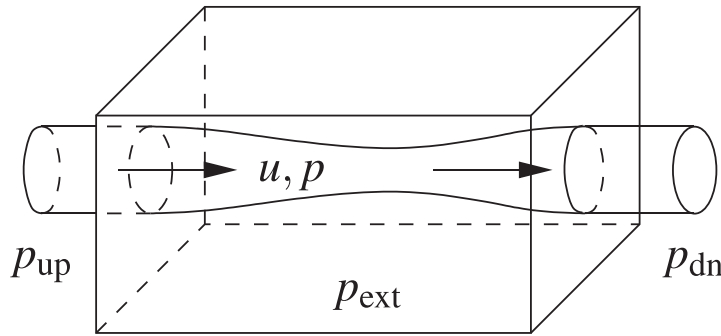
FIG. 1. A schematic diagram of the Starling resistor setup, showing a finite length of elastic-walled tube clamped between two rigid tubes and placed inside a pressure chamber. A fluid flow u is induced through the tubes either by imposing a pressure difference between the ends (as shown) or by using a volumetric pump at one end.

the elastic section has been clamped. Experimental studies using this setup have revealed a rich variety of behaviour, including the growth of large-amplitude self-excited oscillations (see, e.g., Bertram & Tscherry, 2006; Bertram, 2008).

In order to effectively model the fluid–structure interaction in such situations, one needs a description of the mechanics of the elastic tube wall. In many applications, the tube is long compared to its diameter, and the wall is relatively thin. Both of these can be exploited in both ad-hoc and asymptotic modelling.

A common way of modelling the wall mechanics (particularly in the long-wavelength thin-walled limit) is to use a so-called 'tube law'. This is an equation of the form $p = P(A)$ that relates the transmural (interior minus exterior) pressure p at a given axial position to the cross-sectional area A of the tube at that position. Such tube laws have been proposed based on fitting experimental data (e.g. Shapiro, 1977; Kececioglu et al., 1981) and have also been derived theoretically (e.g. Flaherty et al., 1972; McClurken et al., 1981).

More recently, Whittaker et al. (2010) used shell-theory and long-wavelength approximations to derive a tube law for the asymptotic limit of small-amplitude deformations a long thin-walled elastic tube with an initially elliptical cross-section. The resulting tube law took the form

$$p = k_0 A + k_2 \frac{\partial^2 A}{\partial z^2} \tag{1.1}$$

where k_0 and k_2 are numerically determined constants. The two terms in (1.1) arise physically from azimuthal bending and the interaction between axial tension and curvature respectively. Other physical effects are found to be asymptotically small provided we remain in a long-wavelength thin-walled regime.

However, the full set of boundary conditions at the ends of the elastic-walled tube in a Starling resistor setup involves the elastic part being *clamped* to the rigid supports. This means that both the position and gradient of the wall is fixed there. Within the asymptotic model of Whittaker et al. (2010), the normal and azimuthal displacements can be fixed at the ends, but the axial displacement and gradient cannot. This inability to set all the boundary conditions results from the neglect of terms containing higher derivatives in z in the long-wavelength asymptotic regime.

In order to satisfy the remaining boundary conditions, we would expect to find that boundary layers occur near the ends of the tube. Within such layers, a shorter axial length-scale allows some of the neglected effects to re-enter the problem at leading order.

Initial progress in this area was made by Whittaker (2015). To satisfy 'pinned' boundary conditions (in which the position of the tube wall is fixed but not its gradient) the additional physical effect of in-plane shear was found to be needed, resulting in two nested boundary layers. In certain regimes it was found that the boundary layers could have a significant effect on the bulk solution in the main part of the tube. However, this work still did not address the issue of what boundary layers would be needed in order to satisfy fully clamped boundary conditions.

In the present work, we re-analyse the full shell equations for the tube wall in the thin-walled small-deformation limit, and seek distinguished axial length scales that give rise to asymptotic balances in the equations. This leads to the discovery of a number of different boundary layers in three distinct regimes. These boundary layers involve different balances of forces from azimuthal bending, azimuthal hoop stress, the interaction of the axial pre-stress with curvature, the in-plane shear stress, and the applied transmural pressure. In each of the regimes, the solutions in the relevant boundary layers are matched to provide a full solution that is able to satisfy the clamped boundary conditions at the tube end and match to bulk solutions valid over most of the length of the tube.

This paper is organised as follows. In §2 we describe the mathematical setup of the problem and the parameter regimes we shall be considering. In §3 we derive the linearised equilibrium equations that must be satisfied. In §§4–6 we consider the possible asymptotic balances in boundary layers with different axial length scales. In §§7–9 we consider in detail the asymptotic boundary-layer structures in three different regimes. In §10 we validate the asymptotic results by comparing them with an exact solution in a special case. Finally, discussion and conclusions are presented in §11.

2. Mathematical setup and scaling analysis

2.1. *Problem description*

We follow the setup of Whittaker (2015), and consider an elastic-walled tube that is initially an axially uniform elliptical cylinder of axial length L, azimuthal circumference $2\pi a$, and wall thickness d, as shown in Figure 2. The ellipticity of the tube is set by a parameter σ_0 so that the major–minor axis ratio is given by $\coth\sigma_0$. For reasonable ellipticities, a will be the length scale of the semi-axes of the tube's cross-section. The tube wall is made of linearly elastic material with bending stiffness K and Poisson ratio ν. The two ends of the tube are clamped to rigid elliptical supports. In its initial elliptical configuration, the tube is subject to an externally applied uniform axial pre-stress, due to an axial tension F. We then wish to consider deformations induced by an applied transmural pressure p (possibly non-uniform), with dimensional scale P. The dimensional scale for the induced normal deformations in the bulk of the tube is denoted e.

2.2. *Dimensionless parameters and parameter regime*

In general, we shall use the cross-sectional length scale a to non-dimensionalise lengths, and the bending stiffness K to non-dimensionalise stresses. Following Whittaker *et al.* (2010), we introduce the following dimensionless parameters and their asymptotic sizes:

$$\ell = \frac{L}{a} \gg 1, \qquad \vartheta = \frac{d}{a} \ll 1, \qquad \mathscr{F} = \frac{aF}{2\pi K\ell^2} = O(1), \qquad \varepsilon = \frac{e}{a} \ll 1. \tag{2.1}$$
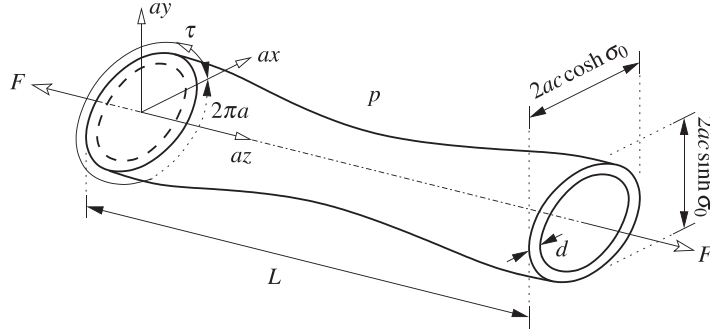
FIG. 2. The general setup of the elastic-walled tube. The tube has length L, wall-thickness d, and an initially elliptical cross-section with semi-axes $ac\cosh\sigma_0$ and $ac\sinh\sigma_0$ and a circumference of $2\pi a$. The tube is subject to an axial tension F and a transmural pressure p. Also shown are the dimensionless Cartesian coordinates x, y, z. The dimensionless coordinate $\tau \in [0, 2\pi)$ is the elliptical angle around the circumference, rather than arclength.

The parameters ℓ and ϑ are aspect ratios, assumed to be large and small respectively for a long thin-walled tube. $\mathscr{F}$ is a dimensionless measure of the axial tension, taken to be $O(1)$ so that the restoring force from the axial tension has the same magnitude as the restoring force from azimuthal bending of the tube wall. The parameter ε measures the dimensionless amplitude of the deformations induced by the pressure. We assume $\varepsilon \ll 1$, so that all $O(\varepsilon^2)$ terms can be neglected, allowing us to linearise the problem for small amplitude perturbations.

It will also be convenient to introduce the additional parameter

$$\tilde{\mathscr{F}} = \frac{\vartheta^2 \ell^2 \mathscr{F}}{12(1 - \nu^2)}, \tag{2.2}$$

which will appear naturally in the asymptotic equations below. In this work we consider only the case where $\vartheta\ell \ll 1$, so that $\tilde{\mathscr{F}} \ll 1$.

In our linearised problem, the size of the deformations (and hence ε) is proportional to the pressure scale P. The constant of proportionality depends on the dominant mechanics in the coupling between the pressure and the deformations. This in turn depends on the precise parameter regime. In this work, we consider three distinct regimes, referred to as Regimes Ia, Ib and Iab. As we shall see below in §4, appropriate expressions for ε are:

$$\varepsilon = \begin{cases} \dfrac{a^3 P}{K} & : \quad \text{Regime Ia} \\[3mm] \dfrac{a^3 \vartheta^3 \ell P}{K \tilde{\mathscr{F}}^{3/2}} & : \quad \text{Regimes Ib and Iab} \end{cases} \tag{2.3}$$

The first expression follows Whittaker (2015); the second is derived here in Appendix C.

2.3. *Coordinates for the tube wall and deformation*

We describe the deformed position of the tube wall parametrically by $r(\tau, z)$. Motivated by an elliptical cylindrical coordinate system, we take τ and z to be dimensionless material coordinates, defined so that

the position of the undeformed tube wall is is given by

$$\bar{r}(\tau,z) = a \begin{pmatrix} c \cosh \sigma_0 \cos \tau \\ c \sinh \sigma_0 \sin \tau \\ z \end{pmatrix} . \tag{2.4}$$

The coordinates therefore lie in the ranges $\tau \in (0, 2\pi)$ and $z \in (0, \ell)$. The dimensionless constant c is given by

$$c = \frac{\pi \operatorname{sech} \sigma_0}{2 \operatorname{Ee}(\operatorname{sech} \sigma_0)}, \tag{2.5}$$

so that the circumference of the undeformed tube is precisely $2\pi a$. (Here $\operatorname{Ee}(k)$ is the complete elliptic integral of the second kind, given by $\operatorname{Ee}(k) \equiv \int_0^{\pi/2} \sqrt{1 - k^2 \sin^2 \theta} \, d\theta$.)

We also define unit vectors $\hat{t}$ and $\hat{z}$ aligned respectively with the τ and z coordinates in the undeformed surface, and a unit vector $\hat{n}$ normal to the undeformed surface. Following Whittaker *et al.* (2010), we introduce the scale factor

$$h(\tau) = \frac{1}{a} \left| \frac{\partial \bar{r}}{\partial \tau} \right| = c \left(\tfrac{1}{2} \cosh 2\sigma_0 - \tfrac{1}{2} \cos 2\tau \right)^{1/2}. \tag{2.6}$$

The unit vectors are then given by

$$\hat{t} = \frac{1}{ah} \frac{\partial \bar{r}}{\partial \tau}, \qquad \hat{z} = \frac{1}{a} \frac{\partial \bar{r}}{\partial z}, \qquad \hat{n} = \hat{t} \times \hat{z}. \tag{2.7}$$

For later use, we also define the dimensionless base-state azimuthal curvature by

$$\bar{B} \equiv \hat{n} \cdot \frac{1}{h} \frac{\partial \hat{t}}{\partial \tau} = -\frac{c^2 \sinh 2\sigma_0}{2h^3}. \tag{2.8}$$

We adopt the same representation of the wall displacements as in Whittaker (2015), namely

$$r - \bar{r} = \frac{\varepsilon a}{\ell} \left(\frac{1}{h(\tau)} \left[\xi(\tau,z)\hat{n} + \eta(\tau,z)\hat{t} \right] + \zeta(\tau,z)\hat{z} \right), \tag{2.9}$$

where the functions (ξ, η, ζ) describe the dimensionless displacements in the normal, azimuthal and axial directions, respectively. (Note that the $\varepsilon a/\ell$ in the pre-factor in (2.9) means that we need $\xi = O(\ell)$ in the bulk of the tube. This choice of scaling may appear slightly unconventional, but is used here for consistency with Whittaker (2015).)

The clamped boundary conditions at the tube ends imply that

$$r(\tau,z) = \bar{r}(\tau,z) \quad \text{and} \quad \hat{n} \cdot \frac{\partial r}{\partial z}(\tau,z) = 0 \quad \text{at} \quad z = 0, \ell. \tag{2.10}$$

In terms of the dimensionless functions in (2.9), these boundary conditions correspond to

$$\xi = 0, \qquad \frac{\partial \xi}{\partial z} = 0, \qquad \eta = 0, \qquad \zeta = 0. \tag{2.11}$$

Standard periodic boundary conditions apply at $\tau = 0$ and $\tau = 2\pi$.

3. Equilibrium equations

In the absence of tangential and axial forces on the wall, and of wall inertia, the Kirchhoff–Love shell equations used by Whittaker *et al.* (2010) to model the wall displacements are

$$\nabla_\alpha \nabla_\beta M^{\alpha\beta} + N^{\alpha\beta} b_{\alpha\beta} = -p, \tag{3.1}$$

$$\nabla_\beta N^{\beta 1} - b^1_\gamma \nabla_\beta M^{\beta\gamma} = 0, \tag{3.2}$$

$$\nabla_\beta N^{\beta 2} - b^2_\gamma \nabla_\beta M^{\beta\gamma} = 0. \tag{3.3}$$

where $b_{\alpha\beta}$ is the curvature tensor, $N^{\alpha\beta}$ is the in-plane stress tensor, $M^{\alpha\beta}$ is the bending moment tensor, and ∇_α is the covariant derivative in the direction x^α. The Greek letter indices range over $(1,2)$, for two in-plane directions, and the summation convention is adopted. As in Whittaker *et al.* (2010), we take the material coordinates x^α to satisfy $\mathrm{d}x^1 = ah(\tau)\,\mathrm{d}\tau$ and $\mathrm{d}x^2 = a\,\mathrm{d}z$, so they are aligned with the tube geometry in the undeformed state. Following the usual convention, subscript and superscript indices represent covariant and contravariant tensor components respectively. Indices can be raised or lowered using the metric tensor $a_{\alpha\beta}$ (defined in (A.2)), so e.g. $b_{\alpha\gamma} = a_{\alpha\beta} b^\beta_\gamma$.

The curvature tensor $b_{\alpha\beta}$ is obtained geometrically from the displacements, while the stresses $N^{\alpha\beta}$ and $M^{\alpha\beta}$ are related to the displacements through the elastic constitutive law, which we assume to be linear. Following Whittaker (2015), we obtain leading-order expressions for these tensors in terms of the displacement functions (ξ, η, ζ). The detailed calculations can be found in Appendix A. We obtain

$$b_{\alpha\beta} = \frac{\bar{B}}{a} \begin{pmatrix} 1 & 0 \\ 0 & 0 \end{pmatrix} + \frac{\varepsilon}{a\ell h} \begin{pmatrix} \tilde{b}_{11} & \tilde{b}_{12} \\ \tilde{b}_{21} & \tilde{b}_{22} \end{pmatrix} + O\left(\frac{\varepsilon}{a\ell} \cdot \frac{\varepsilon}{\ell}\right), \tag{3.4}$$

$$N^{\alpha\beta} = \frac{K}{a^2} \begin{pmatrix} 0 & 0 \\ 0 & \ell^2 \mathscr{F} \end{pmatrix} + \frac{\varepsilon K}{a^2 \vartheta^2 \ell} \begin{pmatrix} \tilde{N} & \tilde{S} \\ \tilde{S} & \tilde{\Sigma} \end{pmatrix} + O\left(\frac{\varepsilon K}{a^2 \vartheta^2 \ell}\left(\vartheta^2, \frac{\varepsilon}{\ell}\right)\right), \tag{3.5}$$

$$M^{\alpha\beta} = \frac{\varepsilon K}{a\ell} \begin{pmatrix} \tilde{M}^{11} & \tilde{M}^{12} \\ \tilde{M}^{21} & \tilde{M}^{22} \end{pmatrix} + O\left(\frac{\varepsilon K}{a\ell} \cdot \frac{\varepsilon}{\ell}\right), \tag{3.6}$$

in terms of the dimensionless curvature components $\tilde{b}_{\alpha\beta}$, the dimensionless azimuthal hoop stress $\tilde{N}$, the dimensionless in-plane shear stress $\tilde{S}$, the dimensionless axial stress perturbation $\tilde{\Sigma}$, and the dimensionless bending moments $\tilde{M}^{\alpha\beta}$ (all functions of τ and z).

The leading-order dimensionless curvature components are

$$\tilde{b}_{11} = \bar{B}\left(-\xi\bar{B} + \frac{\partial}{\partial\tau}\left(\frac{\eta}{h}\right)\right) + \frac{\partial}{\partial\tau}\left(\frac{\eta\bar{B}}{h} + \frac{1}{h}\frac{\partial}{\partial\tau}\left(\frac{\xi}{h}\right)\right), \tag{3.7}$$

$$\tilde{b}_{12} = \tilde{b}_{21} = \frac{\partial^2}{\partial r\partial z}\left(\frac{\xi}{h}\right) + \bar{B}\frac{\partial\eta}{\partial z}, \tag{3.8}$$

$$\tilde{b}_{22} = \frac{\partial^2\xi}{\partial z^2}; \tag{3.9}$$

the leading-order dimensionless in-plane stress components are

$$\tilde{N} = 12\left(-\frac{\bar{B}\xi}{h} + \frac{1}{h}\frac{\partial}{\partial\tau}\left(\frac{\eta}{h}\right) + \nu\frac{\partial\zeta}{\partial z}\right), \tag{3.10}$$

$$\tilde{S} = \frac{12(1-\nu)}{2h}\left(\frac{\partial\eta}{\partial z} + \frac{\partial\zeta}{\partial\tau}\right), \tag{3.11}$$

$$\tilde{\Sigma} = 12\left(\frac{\partial\zeta}{\partial z} + \nu\left(-\frac{\bar{B}\xi}{h} + \frac{1}{h}\frac{\partial}{\partial\tau}\left(\frac{\eta}{h}\right)\right)\right); \tag{3.12}$$

and the leading-order dimensionless bending moments are

$$\tilde{M}^{11} = \bar{B}\left(-\frac{\xi\bar{B}}{h} + \frac{1}{h}\frac{\partial}{\partial\tau}\left(\frac{\eta}{h}\right)\right) - \frac{1}{h}\frac{\partial}{\partial\tau}\left(\frac{\eta\bar{B}}{h} + \frac{1}{h}\frac{\partial}{\partial\tau}\left(\frac{\xi}{h}\right)\right) - \nu\frac{\partial^2}{\partial z^2}\left(\frac{\xi}{h}\right), \tag{3.13}$$

$$\tilde{M}^{12} = \frac{(1-\nu)}{h}\left[-\frac{\partial^2}{\partial\tau\partial z}\left(\frac{\xi}{h}\right) + \frac{\bar{B}}{2}\left(\frac{\partial\zeta}{\partial\tau} - \frac{\partial\eta}{\partial z}\right)\right], \tag{3.14}$$

$$\tilde{M}^{21} = \frac{(1-\nu)}{h}\left[-\frac{\partial^2}{\partial\tau\partial z}\left(\frac{\xi}{h}\right) + \bar{B}\frac{\partial\zeta}{\partial\tau}\right], \tag{3.15}$$

$$\tilde{M}^{22} = \bar{B}\frac{\partial\zeta}{\partial z} + 2\nu\bar{B}\left(-\frac{\xi\bar{B}}{h} + \frac{1}{h}\frac{\partial}{\partial\tau}\left(\frac{\eta}{h}\right)\right)$$
$$- \frac{\partial^2}{\partial z^2}\left(\frac{\xi}{h}\right) - \frac{\nu}{h}\frac{\partial}{\partial\tau}\left(\frac{\eta\bar{B}}{h} + \frac{1}{h}\frac{\partial}{\partial\tau}\left(\frac{\xi}{h}\right)\right). \tag{3.16}$$

From Whittaker (2015), the covariant derivatives ∇_α are given by

$$\nabla_1 = \frac{1}{ah}\frac{\partial}{\partial\tau} + O(\varepsilon), \quad \nabla_2 = \frac{1}{a}\frac{\partial}{\partial z} + O(\varepsilon). \tag{3.17}$$

As in Whittaker (2015), the only place we need to include the $O(\varepsilon)$ correction terms in (3.17) is where the derivatives are applied to the large axial pre-stress in N^{22}. The relevant expression is

$$\nabla_\alpha N^{\alpha\beta} = \frac{\partial N^{\alpha\beta}}{\partial x^\alpha} + \Gamma^\alpha_{\gamma\alpha}N^{\gamma\beta} + \Gamma^\beta_{\gamma\alpha}N^{\alpha\gamma}, \tag{3.18}$$

where

$$\Gamma^1_{21} = \frac{1}{a}\frac{\partial\gamma_{11}}{\partial z}, \qquad \Gamma^1_{22} = \frac{\varepsilon}{a\ell h}\frac{\partial^2\eta}{\partial z^2}, \qquad \Gamma^2_{22} = \frac{\varepsilon}{a\ell}\frac{\partial^2\zeta}{\partial z^2}, \tag{3.19}$$

and γ_{11} is a component of the in-plane shear, as defined in (A.3) and expressed in terms of ξ and η in (A.15). Finally, we introduce a non-dimensional pressure $\tilde{p}$, by writing

$$p = P\tilde{p}. \tag{3.20}$$

Substituting the above expressions into (3.1)–(3.3), and neglecting terms of $O(\varepsilon^2)$, we obtain the following equilibrium equations:

$$\vartheta^2\left(\tilde{M}_{\tau\tau}^{11}+\tilde{M}_{\tau z}^{12}+\tilde{M}_{z\tau}^{21}+\tilde{M}_{zz}^{22}\right)+\bar{B}\tilde{N}+12(1-\nu^2)\tilde{\mathscr{F}}\left(\frac{\xi}{h}\right)_{zz} = -\mathscr{P}\,\tilde{p}, \qquad (3.21)$$

$$\left(\tilde{N}_{\tau}+\tilde{S}_z\right)+12(1-\nu^2)\tilde{\mathscr{F}}\left(\frac{\eta}{h}\right)_{zz}-\vartheta^2\bar{B}\left(\tilde{M}_{\tau}^{11}+\tilde{M}_z^{21}\right) = 0, \qquad (3.22)$$

$$\left(\tilde{S}_{\tau}+\tilde{\Sigma}_z\right)+12(1-\nu^2)\tilde{\mathscr{F}}\left[-\left(\frac{\xi\bar{B}}{h}\right)_z+\left(\frac{\eta}{h}\right)_{\tau z}+2\zeta_{zz}\right] = 0, \qquad (3.23)$$

where $\tilde{N}$, $\tilde{S}$, $\tilde{\Sigma}$ and $\tilde{M}^{\alpha\beta}$ are given by (3.10)–(3.16), $(\cdot)_z \equiv \partial/\partial z$, $(\cdot)_{\tau} \equiv h^{-1}\partial/\partial\tau$, and the pressure scale $\mathscr{P}$ is given by

$$\mathscr{P} = \frac{\vartheta^2\ell a^3 P}{\varepsilon K}. \qquad (3.24)$$

The size of $\mathscr{P}$ is fixed by the relationship between ε and P, which will be determined in §4 below. The boundary conditions on the system are (2.11) at $z=0$ and $z=\ell$, together with periodic conditions between $\tau=0$ and $\tau=2\pi$.

For $\vartheta \ll 1$ and $\tilde{\mathscr{F}} \ll 1$, the highest axial derivatives in each of the equations (3.21)–(3.23) are multiplied by small parameters, so we expect to find boundary layers. We wish to find a matched asymptotic solution to (3.21)–(3.23) and (2.11) involving boundary layers of different thicknesses in the axial z direction. To find the possible boundary-layer widths δ, we consider possible balances in the equations when $z = O(\delta)$. (The scalings are such that $\delta = 1$ corresponds to a thickness in z of the same order as the diameter of the tube, while $\delta = \ell$ corresponds to the length of the tube.) We compile table 1, which gives the sizes and origins of the various terms in the equilibrium equations (3.21)–(3.23) when $z = O(\delta) \lesssim 1$. In the sections that follow, we shall use this table to consider the dominant balances at different magnitudes of δ that give rise to different boundary layers in the region of parameter space where $\vartheta \ll 1$ and $\tilde{\mathscr{F}} \ll 1$.

4. Analysis for $\delta \gg 1$

For a boundary-layer of width $\delta \gg 1$, we make use of the analysis in Whittaker (2015), where a 'bulk solution' with $\delta = O(\ell)$ and an 'outer shear layer' with $\delta = O(\tilde{\mathscr{F}}^{-1/2})$ are found. The analysis there must be adapted for our case here, in two different ways depending on the precise regime.

When $\tilde{\mathscr{F}}^{-1/2} \ll \ell$, we expect the same boundary-layer structure for the outer shear layer as in Whittaker (2015). The bulk solution is forced directly by the transmural pressure, which is balanced by azimuthal bending and axial pre-stress/curvature effects. The structure of the outer shear layer is primarily set by a balance between between the axial stress and axial pre-stress/curvature effects. In both the outer shear layer and the bulk, azimuthal hoop stress and in-plane shear stress are also present at leading order. The transmural pressure does not appear directly in the equations for the outer shear layer. Instead the displacements there are forced by the matching of this layer to the bulk solution.

The inner boundary conditions on the outer shear layer that we need here are different from those in Whittaker (2015), as we expect a different boundary-layer structure for $\delta \lesssim 1$. The details of the outer shear layer when $\tilde{\mathscr{F}}^{-1/2} \ll \ell$ can be found in Appendix B below, where a solution is derived in terms of the azimuthal eigenfunctions $Y_n(\tau)$ of a particular linear operator. The relationship between the size

Physical Effect	Contribution to Normal Balance (3.21)	Contribution to Azimuthal Balance (3.22)	Contribution to Axial Balance (3.23)
Hoop Stress	$\bar{B}\tilde{N} \sim (\xi, \eta, \zeta/\delta)$	$\tilde{N}_\tau \sim (\xi, \eta, \zeta/\delta)$	
Shear Stress	—	$\tilde{S}_z \sim (\eta/\delta^2, \zeta/\delta)$	$\tilde{S}_\tau \sim (\eta/\delta, \zeta)$
Axial Stress	—		$\tilde{\Sigma}_z \sim (\xi/\delta, \eta/\delta, \zeta/\delta^2)$
Pre-Stress/ Curvature	$\tilde{\mathscr{F}}\xi_{zz} \sim \tilde{\mathscr{F}}\xi/\delta^2$	$\tilde{\mathscr{F}}\eta_{zz} \sim \tilde{\mathscr{F}}\eta/\delta^2$	$\tilde{\mathscr{F}}(\gamma_{11_z} + \zeta_{zz})$ $\sim$ $\tilde{\mathscr{F}}(\xi/\delta, \eta/\delta, \zeta/\delta^2)$
Azimuthal Bending	$\vartheta^2(\tilde{M}^{11})_{\tau\tau}$ $\sim \vartheta^2(\xi, \xi/\delta^2, \eta)$	$\vartheta^2\bar{B}(\tilde{M}^{11})_\tau$ $\sim \vartheta^2(\xi, \xi/\delta^2, \eta)$	—
Torsion	$\vartheta^2\big((\tilde{M}^{12})_{\tau z} + (\tilde{M}^{21})_{z\tau}\big)$ $\sim \vartheta^2(\xi/\delta^2, \eta/\delta^2, \zeta/\delta)$	$\vartheta^2\bar{B}(\tilde{M}^{21})_z$ $\sim \vartheta^2(\xi/\delta^2, \zeta/\delta)$	—
Axial Bending	$\vartheta^2(\tilde{M}^{22})_{zz}$ $\sim \vartheta^2(\xi, \xi/\delta^2, \eta, \zeta/\delta)/\delta^2$	—	—
Transmural Pressure	$\mathscr{P}$	—	—

TABLE 1 *Scale estimates of the dimensionless contributions to the dimensionless equilibrium equations (3.21)–(3.23) from the different physical effects, over an arbitrary axial length scale $z \sim \delta$, where $\delta \lesssim 1$. (All three equations have been non-dimensionalised on the common scale $\varepsilon K/(a^3 \ell \vartheta^2)$, and the axial coordinate z has been non-dimensionalised using the length scale a of the tube cross-section.)*

of the deformations and the pressure scale is as found by Whittaker (2015), so we have

$$\varepsilon = \frac{a^3 P}{K} \qquad \Rightarrow \qquad \mathscr{P} = \vartheta^2 \ell. \tag{4.1}$$

For $\tilde{\mathscr{F}}^{-1/2} \gtrsim \ell$ on the other hand, the outer shear layer extends to the whole of the length of the tube, and there is no separate bulk solution. The forcing of the displacements in this single 'bulk shear layer' must come directly from the transmural pressure acting within that layer. The displacements must therefore be smaller, so that the transmural pressure appears at leading-order in the equations for the bulk shear layer. The relevant calculations can be found in Appendix C below, where the solution is constructed in terms of the same azimuthal eigenfunctions $Y_n(\tau)$. We find that, at leading-order, the applied transmural pressure is balanced by the combination of all three in-plane stresses. The relationship between the size of the deformations and the pressure scale is found to be

$$\varepsilon = \frac{\vartheta^2 \ell^4 a^3 P}{K} \qquad \Rightarrow \qquad \mathscr{P} = \ell^{-3}. \tag{4.2}$$

5. Analysis for $\delta = O(1)$

We refer to table 1 and consider $\delta = O(1)$. Following our chosen parameter regime (2.1), we take $\vartheta \ll 1$, $\tilde{\mathscr{F}} \ll 1$ and $\mathscr{F} = O(1)$. We also assume that the $O(\mathscr{P})$ contribution from transmural pressure

in (3.21) is negligible at this axial length scale. (This is appropriate since the pressure is forcing the displacements in a region with a longer axial length scale. The shorter length scale here will increase the magnitude of some of the other terms in the equilibrium equations, meaning that the pressure no longer contributes to the leading-order balances.)

When $\delta = O(1)$ we have equal axial and azimuthal length-scales. This suggests that the three displacements (ξ, η, ζ) should all have the same scaling, which also leads to the principal stresses $(\tilde{N}, \tilde{S}, \tilde{\Sigma})$ having this same expected scaling too. We define $\mathscr{C}$ to be this common scale. Since the equations we are considering are linear and homogeneous, the common scaling is arbitrary as far as the equations are concerned. It will instead be determined by the matching conditions. It will turn out that appropriate choices will be $\mathscr{C} = \tilde{\mathscr{F}}^{1/2}$ when $\vartheta \ll \tilde{\mathscr{F}} \ll 1$ (Regime Ia) and $\mathscr{C} = \ell^{-1}$ when $\tilde{\mathscr{F}} \lesssim \vartheta \ll 1$ (Regimes Ib and Iab), both of which satisfy $\mathscr{C} \ll 1$.

5.1. *Dominant balances in the equilibrium equations*

Referring to table 1, we first consider the normal balance (3.21). Since $\vartheta \ll 1$, $\tilde{\mathscr{F}} \ll 1$ and $\delta = O(1)$, the hoop-stress term $\bar{B}\tilde{N}$ dominates (3.21). With no other terms at this order, $\tilde{N}$ must vanish at its $O(\mathscr{C})$ expected order. In other words, the various $O(\mathscr{C})$ contributions to $\tilde{N}$ from the displacements cancel between themselves at this order. The actual size of $\tilde{N}$ is then set by the maximum size of the other terms in (3.21): $O(\vartheta^2 \mathscr{C})$, $O(\tilde{\mathscr{F}}\mathscr{C})$ and $O(\mathscr{P})$. The definition (2.2) gives $\tilde{\mathscr{F}} \sim \ell^2 \vartheta^2 \mathscr{F}$, and we have assumed that $\mathscr{F} = O(1)$ and $\ell \gg 1$. Therefore, $\vartheta^2 \ll \tilde{\mathscr{F}}$, and hence $\tilde{N}$ is at least a factor of $O(\tilde{\mathscr{F}}, \mathscr{C}^{-1}\mathscr{P})$ smaller than its $O(\mathscr{C})$ anticipated scale.

In the azimuthal balance (3.22), the hoop stress $\tilde{N}_\tau$ and shear stress $\tilde{S}_z$ would be present at leading order if they both had their expected $O(\mathscr{C})$ magnitudes. However, $\tilde{N}_\tau$ vanishes at that order. Hence we have $\tilde{S}_z = 0$ at its $O(\mathscr{C})$ expected order, with non-zero corrections coming in only at a relative $O(\tilde{\mathscr{F}}, \mathscr{C}^{-1}\mathscr{P})$ smaller.

In the axial balance (3.23), the shear stress $\tilde{S}_\tau$ and axial stress $\tilde{\Sigma}_z$ are present at leading order, with an $O(\mathscr{C})$ magnitude. However, $\tilde{S}_{\tau z}$ must vanish at that order. So, taking the z derivative of (3.23), we have that $\tilde{\Sigma}_{zz} = 0$ at its $O(\mathscr{C})$ expected order, with non-zero corrections coming in only at a relative $O(\tilde{\mathscr{F}}, \mathscr{C}^{-1}\mathscr{P})$ smaller.

5.2. *Form of the stress components*

Based on the above arguments, we can write the stress components as

$$\tilde{N} = \mathscr{C}\left[0 + O(\tilde{\mathscr{F}}, \mathscr{C}^{-1}\mathscr{P})\right], \tag{5.1}$$

$$\tilde{S} = \frac{\mathscr{C}}{2(1+\nu)h(\tau)}\left[\left(A_0(\tau) + \mathscr{C}A_1(\tau)\right) + O(\tilde{\mathscr{F}}, \mathscr{C}^{-1}\mathscr{P})\right], \tag{5.2}$$

$$\tilde{\Sigma} = \mathscr{C}\left[\left(B_0(\tau)z + C_0(\tau)\right) + \mathscr{C}\left(B_1(\tau)z + C_1(\tau)\right) + O(\tilde{\mathscr{F}}, \mathscr{C}^{-1}\mathscr{P})\right], \tag{5.3}$$

where A_i, B_i and C_i are arbitrary $O(1)$ functions of τ, and the denominator in the expression for $\tilde{S}$ is chosen for later convenience. The $i = 1$ functions are included because we know that the expression (5.2) will need to be matched to (B.5) in the outer shear layer or (C.16) in the bulk shear layer. Both (B.5) and (C.16) turn out to have magnitudes equivalent to $O(\mathscr{C}^2)$, and so may induce $O(\mathscr{C}^2)$ corrections in (5.2).

Substituting the forms (5.1)–(5.3) into the equilibrium equations (3.21)–(3.23), we find that the normal balance (3.21) and the azimuthal balance (3.22) are automatically satisfied to $o(\mathscr{C}\tilde{\mathscr{F}}, \mathscr{P})$ with

no constraints on the functions A_0, B_i and C_i. The axial balance (3.23) however, requires

$$\frac{1}{2(1+v)h}\frac{\partial}{\partial \tau}\left(\frac{A_0}{h}\right)+B_0=0, \qquad \frac{1}{2(1+v)h}\frac{\partial}{\partial \tau}\left(\frac{A_1}{h}\right)+B_1=0. \tag{5.4}$$

This allows us to express B_0 and B_1 in terms of A_0 and A_1, though it is more convenient not to eliminate B_0 and B_1 at this point.

5.3. *Displacement recovery*

Recovering the leading-order displacements from (5.1)–(5.3) using equations (A.34)–(A.36), we obtain

$$\xi = \frac{\mathscr{C}}{12(1-v^2)\bar{B}}\left[vh(B_0z+C_0)-\frac{\partial}{\partial \tau}\left(\frac{\frac{1}{6}B_0'z^3+\frac{1}{2}C_0'z^2-(A_0-D_0')z-E_0}{h}\right)\right], \tag{5.5}$$

$$\eta = \frac{\mathscr{C}}{12(1-v^2)}\left(-\frac{1}{6}B_0'z^3-\frac{1}{2}C_0'z^2+\left(A_0-D_0'\right)z+E_0\right), \tag{5.6}$$

$$\zeta = \frac{\mathscr{C}}{12(1-v^2)}\left(\frac{1}{2}B_0z^2+C_0z+D_0\right), \tag{5.7}$$

where A_0,B_0,C_0 are the arbitrary $O(1)$ functions of τ introduced in (5.1)–(5.3); D_0 and E_0 are additional arbitrary $O(1)$ functions of τ (arising as constants of integration); and a prime denotes differentiation with respect to τ.

6. Analysis for $\delta \ll 1$

We again make use of table 1, and consider balances in a boundary-layer of axial length δ, where $\delta \ll 1$. As before, we take $\vartheta \ll 1$, $\tilde{\mathscr{F}} \ll 1$ and $\mathscr{F} = O(1)$, and assume that the $O(\mathscr{P})$ transmural pressure is negligible at this length scale. (The latter assumption is found to be consistent with the solutions obtained.)

6.1. *Azimuthal balance*

Examining the 'Azimuthal' column of table 1, the possible dominant terms in the azimuthal balance (3.22) are: the $O(\xi)$ and $O(\zeta/\delta)$ contributions from the hoop stress, the $O(\eta/\delta^2)$ and $O(\zeta/\delta)$ contributions from the shear stress, and $O(\vartheta^2\xi/\delta^2)$ contributions from azimuthal bending and torsion. The other terms are all asymptotically smaller than one of these.

We now consider the $O(\eta/\delta^2)$ contribution from the shear stress. If this is asymptotically larger than all the other terms, then η_{zz} itself must vanish at that order. Otherwise there must be other terms in the leading-order balance, in which case we need

$$\eta \lesssim \max\left\{\delta^2\xi,\vartheta^2\xi,\delta\zeta\right\}. \tag{6.1}$$

From the latter we can deduce that

$$\eta \ll \max\left\{\xi,\zeta/\delta\right\}, \tag{6.2}$$

and also

$$\frac{\vartheta^2\eta}{\delta^2} \lesssim \max\left\{\vartheta^2\xi,\vartheta^4\xi/\delta^2,\vartheta^2\zeta/\delta\right\} \ll \max\left\{\xi,\vartheta^2\xi/\delta^2,\zeta/\delta\right\}. \tag{6.3}$$

6.2. *Axial balance*

Examining the 'Axial' column of table 1, the possible dominant terms in the axial balance (3.23) are: the $O(\eta/\delta)$ contribution from the shear stress, and the $O(\xi/\delta)$, $O(\eta/\delta)$ and $O(\zeta/\delta^2)$ contributions from the axial stress.

If (6.2) holds, then we see that the two η terms in (3.23) must be asymptotically smaller than at least one of the other terms. Hence only the $O(\xi/\delta)$ and $O(\zeta/\delta^2)$ contributions from the axial stress can be present at leading order. Considering the $O(\zeta/\delta^2)$ term, we must either have $\zeta_{zz} = 0$ at that order, or else

$$\zeta \lesssim \delta\xi. \tag{6.4}$$

6.3. *Normal balance*

Examining the 'Normal' column of table 1, the possible dominant terms in the normal balance (3.21) are: the $O(\xi)$, $O(\eta)$ and $O(\zeta/\delta)$ contributions from the hoop stress, the $O(\tilde{\mathscr{F}}\xi/\delta^2)$ contribution from the axial pre-stress/curvature, the $O(\vartheta^2\eta/\delta^2)$ contribution from the torsion, and the $O(\vartheta^2\xi/\delta^4)$, $O(\vartheta^2\eta/\delta^2)$ and $O(\vartheta^2\zeta/\delta^3)$ contributions from the axial bending.

If (6.2) holds, we see that the $O(\eta)$ term from the hoop stress is asymptotically smaller than one of the other two hoop stress contributions in (3.21), and so cannot be present in the leading-order balance. Similarly, (6.3) shows that the $O(\vartheta^2\eta/\delta^2)$ contribution from the torsion is always asymptotically smaller than one of the other terms.

If (6.4) holds, we see that the $O(\vartheta^2\zeta/\delta^3)$ term in the axial bending is smaller than the $O(\vartheta^2\xi/\delta^4)$ term in (3.21), so cannot be present at leading order. We also see that that the $O(\zeta/\delta)$ term in the hoop stress is no larger than the $O(\xi)$ term there.

Hence, in the case where (6.1) and (6.4) hold, the possible terms in the leading-order balance are $O(\xi, \zeta/\delta, \tilde{\mathscr{F}}\xi/\delta^2, \vartheta^2\xi/\delta^4)$.

6.4. *Distinguished limits*

We now seek values of δ that could give rise to distinguished limits in the three equilibrium equations, and hence determine the possible boundary-layer thicknesses.

We focus on the normal balance, and start with the case in which (6.1) and (6.4) hold. From §6.3, the possible terms in the leading-order balance are $O(\xi, \zeta/\delta, \tilde{\mathscr{F}}\xi/\delta^2, \vartheta^2\xi/\delta^4)$, and we note that $\zeta \lesssim \delta\xi$ from (6.4). However, if $\zeta \sim \delta\xi$, then the leading-order balance in the axial equation sets the relation between ξ and ζ, which means that we cannot just have the $O(\xi)$ and $O(\zeta/\delta)$ terms alone at leading order in the normal equation. (If this were the case, there would be a second conflicting relation between ξ and ζ.) This means that at least two of the following terms must be present in the normal balance: $O(\xi)$, $O(\tilde{\mathscr{F}}\xi/\delta^2)$, $O(\vartheta^2\xi/\delta^4)$.

Otherwise one or both of (6.1) and (6.4) do not hold. In this case, then at leading order, one of the equations is either $\eta_{zz} = 0$ or $\zeta_{zz} = 0$. We would then have a polynomial solution for the corresponding variable(s), which would appear as a forcing in the remaining equations. Since the system is linear, we can subtract off these polynomials and the corresponding particular integrals for the other variables, leaving behind a system in which (6.1) and (6.4) do both hold. These polynomials and particular integrals cannot give rise to any additional distinguished limits not already occurring in the the system where (6.1) and (6.4) hold.

This means that the normal balance considered above sets the boundary layer widths, via balances between the following components: the hoop stress scaling with ξ, the pre-stress/curvature scaling with $\tilde{\mathscr{F}}\xi/\delta^2$ and the axial bending scaling with $\vartheta^2\xi/\delta^4$. Boundary layers occur when two or more of the
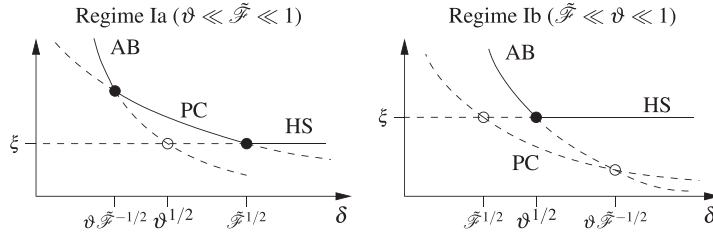
FIG. 3. Sketches of the variation in the scale estimates for the terms in the normal force balance as the axial scale δ varies, showing the distinguished limits (filled circles) in Regimes Ia and Ib. The scales are ξ for the hoop stress (HS), $\tilde{\mathscr{F}}\xi/\delta^2$ for the pre-stress/curvature (PC), and $\vartheta^2\xi/\delta^4$ for the axial bending (AB). Solid lines indicate when these effects are present at leading order; dashed lines are used otherwise. The distinguished limits occur when two of the three effects have the same magnitude, and the third is smaller.

components balance, and any remaining component is asymptotically smaller. Different pairs of these terms balance when $\delta = O(\tilde{\mathscr{F}}^{1/2})$, $\delta = O(\vartheta^{1/2})$ and $\delta = O(\vartheta\tilde{\mathscr{F}}^{-1/2})$. Whether or not the third term is smaller (and hence we have a distinguished limit) in each of these cases is controlled by the relative sizes of ϑ and $\tilde{\mathscr{F}}$, as shown in Figure 3.

For $\vartheta \ll \tilde{\mathscr{F}} \ll 1$, which we term Regime Ia, we have two relevant distinguished limits, which occur at $\delta = O(\vartheta\tilde{\mathscr{F}}^{-1/2})$ and $\delta = O(\tilde{\mathscr{F}}^{1/2})$. Azimuthal bending dominates for $z \ll \vartheta\tilde{\mathscr{F}}^{-1/2}$, pre-stress/curvature for $\vartheta\tilde{\mathscr{F}}^{-1/2} \ll z \ll \tilde{\mathscr{F}}^{1/2}$, and the hoop stress for $\tilde{\mathscr{F}}^{1/2} \ll z$. At $z = O(\vartheta\tilde{\mathscr{F}}^{-1/2})$, we have a balance between the pre-stress/curvature and azimuthal bending, in what we shall term the 'Ia bending layer'. At $z = O(\tilde{\mathscr{F}}^{1/2})$, we have a balance between the hoop stress and the pre-stress/curvature, in what we shall term the 'inner shear layer'.

For $\tilde{\mathscr{F}} \ll \vartheta \ll 1$, which we term Regime Ib, we have only one relevant distinguished limit, which occurs at $\delta = O(\vartheta^{1/2})$. Azimuthal bending dominates for $z \ll \vartheta^{1/2}$, and the hoop stress dominates for $\vartheta^{1/2} \ll z$. At $z = O(\vartheta^{1/2})$, we have a balance between the hoop stress and azimuthal bending, in what we shall term the 'Ib bending layer'. In this regime, the pre-stress/curvature effects are always smaller, and never contribute at leading order.

For $\tilde{\mathscr{F}} \sim \vartheta \ll 1$, which we term Regime Iab, there is one special distinguished limit. This occurs at $\delta = O(\vartheta^{1/2}) = O(\tilde{\mathscr{F}}^{1/2}) = O(\vartheta\tilde{\mathscr{F}}^{-1/2})$, where all three terms are present at leading order. As in Regime Ib, azimuthal bending dominates for $z \ll \tilde{\mathscr{F}}^{1/2}$, and the hoop stress dominates for $\tilde{\mathscr{F}}^{1/2} \ll z$. The difference here is that pre-stress/curvature is also present at $z = O(\tilde{\mathscr{F}}^{1/2})$.

(The Regime nomenclature comes from Walters (2016), where a 'Regime II' with $\tilde{\mathscr{F}} \gg 1$ was also considered. Consideration of that regime, in which shell theory no longer applies in the bending boundary layer, is beyond the scope of this paper.)

7. Regime Ia ($\vartheta \ll \tilde{\mathscr{F}} \ll 1$)

We now consider in detail the boundary layers that exist in Regime Ia, where $\vartheta \ll \tilde{\mathscr{F}} \ll 1$. The governing equations in each layer are derived and solved at leading order, and then the individual boundary-layer solutions are matched to give a full solution. In this regime, we have $\vartheta \ll \tilde{\mathscr{F}}$, which implies $\tilde{\mathscr{F}}^{-1/2} \ll \ell$. Hence, from the analysis of §4, we have an outer shear layer for $z = O(\tilde{\mathscr{F}}^{-1/2})$ and a bulk solution for $z = O(\ell)$. From (4.1), we have $\varepsilon = a^3 P/K$ and $\mathscr{P} = \vartheta^2\ell$. The intermediate region at $z = O(1)$ was considered in §5. Here we consider the expected layers for $z \ll 1$, as anticipated in

§6.4, namely an inner shear layer at $z = O(\tilde{\mathscr{F}}^{1/2})$ and Ia bending layer at $z = O(\vartheta\tilde{\mathscr{F}}^{-1/2})$. We will then complete the matching between the various boundary layers.

7.1. *Inner shear layer* $z = O(\tilde{\mathscr{F}}^{1/2})$

In the inner shear layer with $\delta = \tilde{\mathscr{F}}^{1/2}$, we expect a dominant balance in the normal direction between the azimuthal hoop stress and the pre-stress/curvature terms, with ξ present in both these terms at leading order. We then take $\zeta \sim \delta\xi$ (the largest permitted scale for ζ) so that ζ can also contribute to the hoop stress. For η, the magnitude is constrained by (6.2)–(6.3), meaning it is absent from the normal and axial balances. We thus take $\eta \sim \delta\zeta$ to allow a contribution to the shear stress in the azimuthal balance.

With the relative sizes of ξ, η, and ζ fixed, the only remaining degree of freedom in the scalings is the overall scaling of the displacement amplitudes. This is arbitrary as far as the equations are concerned, as they are linear and homogeneous at leading-order. The magnitude will be set by the matching later on. Nevertheless, it is convenient to chose the right scaling now to simplify the matching below. It turns out that $\xi = O(\tilde{\mathscr{F}}^{1/2})$ is appropriate, to match the magnitude of the small-z limit of (5.5).

We therefore introduce the $O(1)$ scaled variables $\{\hat{z}, \hat{\xi}, \hat{\eta}, \hat{\zeta}\}$, and write:

$$z = \tilde{\mathscr{F}}^{1/2}\hat{z}, \qquad \xi = \tilde{\mathscr{F}}^{1/2}\hat{\xi}, \qquad \eta = \tilde{\mathscr{F}}^{3/2}\hat{\eta}, \qquad \zeta = \tilde{\mathscr{F}}\hat{\zeta}. \tag{7.1}$$

Substituting these expressions into the equilibrium equations (3.21)–(3.23), we obtain the following leading-order equations for the inner shear layer:

$$\bar{B}\left(-\bar{B}\hat{\xi} + \nu h\frac{\partial\hat{\zeta}}{\partial\hat{z}}\right) + (1-\nu^2)\frac{\partial^2\hat{\xi}}{\partial\hat{z}^2} = 0, \tag{7.2}$$

$$\frac{\partial}{\partial\tau}\left(-\frac{2\bar{B}}{h}\hat{\xi} + (1+\nu)\frac{\partial\hat{\zeta}}{\partial\hat{z}}\right) + (1-\nu)\frac{\partial^2\hat{\eta}}{\partial\hat{z}^2} = 0, \tag{7.3}$$

$$\frac{\partial^2\hat{\zeta}}{\partial\hat{z}^2} - \frac{\nu\bar{B}}{h}\frac{\partial\hat{\xi}}{\partial\hat{z}} = 0, \tag{7.4}$$

with neglected terms of $O(\vartheta^2\tilde{\mathscr{F}}^{-2}, \tilde{\mathscr{F}})$, $O(\tilde{\mathscr{F}})$, and $O(\tilde{\mathscr{F}})$, respectively.

Eliminating $\hat{\zeta}$ between (7.2) and (7.4) we obtain

$$\frac{\partial^3\hat{\xi}}{\partial\hat{z}^3} - \bar{B}^2\frac{\partial\hat{\xi}}{\partial\hat{z}} = 0. \tag{7.5}$$

The general solution of (7.5) is

$$\hat{\xi} = \hat{A}e^{-|\bar{B}|\hat{z}} + \hat{B}e^{|\bar{B}|\hat{z}} + \hat{C}, \tag{7.6}$$

where $\hat{A}$, $\hat{B}$, and $\hat{C}$ are arbitrary functions of τ.

Substituting this into (7.2) and integrating, we then find

$$\hat{\zeta} = \frac{\nu}{h}\left(\hat{A}e^{-|\bar{B}|\hat{z}} - \hat{B}e^{|\bar{B}|\hat{z}} + \frac{\bar{B}}{\nu^2}\hat{C}\hat{z} + \hat{D}\right), \tag{7.7}$$

where $\hat{D}$ is another arbitrary function of τ, and we have used the fact that $\bar{B} < 0$.

Substituting (7.6) and (7.7) into (7.3) and integrating, we obtain

$$\hat{\eta} = \frac{\partial}{\partial \tau} \left[\frac{(2+\nu)}{h\bar{B}} \left(\hat{A} \mathrm{e}^{-|\bar{B}|\hat{z}} + \hat{B} \mathrm{e}^{|\bar{B}|\hat{z}} \right) - \frac{\bar{B}}{2\nu h} \hat{C} \hat{z}^2 \right] + \hat{E}\hat{z} + \hat{F}, \tag{7.8}$$

where $\hat{E}$ and $\hat{F}$ are two more arbitrary functions of τ.

Finally, we can use (3.11) to evaluate the shear stress as

$$\begin{aligned}
\tilde{S} &= \tilde{\mathscr{F}} \frac{12(1-\nu)}{2h} \left(\frac{\partial \hat{\eta}}{\partial \hat{z}} + \frac{\partial \hat{\zeta}}{\partial \tau} \right) \\
&= \tilde{\mathscr{F}} \frac{12(1-\nu)}{2h} \left[\frac{\partial}{\partial \tau} \left(\frac{2(1+\nu)}{h} \left(\hat{A} \mathrm{e}^{-|\bar{B}|\hat{z}} - \hat{B} \mathrm{e}^{|\bar{B}|\hat{z}} \right) + \frac{\nu \hat{D}}{h} \right) + \hat{E} \right].
\end{aligned} \tag{7.9}$$

This will be required for the matching below.

7.2. *Ia bending layer $z = O(\vartheta \tilde{\mathscr{F}}^{-1/2})$*

In the Ia bending layer, we expect a dominant balance in the normal direction between the axial bending and the pre-stress/curvature terms. This sets the $O(\vartheta \tilde{\mathscr{F}}^{-1/2})$ boundary-layer width. The appropriate scales for the three displacements arise from the matching with the inner shear layer from §7.1. Linear behaviour of the displacements in the matching region leads to $\xi = O(\vartheta \tilde{\mathscr{F}}^{-1/2})$, $\eta = O(\vartheta \tilde{\mathscr{F}}^{1/2})$ and $\zeta = O(\vartheta)$. (These scales mean that sizes of η and ζ relative to ξ are larger than the maximums envisaged in §6.1 and §6.2. So the alternative options of $\eta_{zz} = 0$ and $\zeta_{zz} = 0$ for the azimuthal and axial balances come in to play.)

We introduce the $O(1)$ scaled variables $\{\check{z}, \check{\xi}, \check{\eta}, \check{\zeta}\}$, and write

$$z = \frac{\vartheta \tilde{\mathscr{F}}^{-1/2} \check{z}}{\sqrt{12(1-\nu^2)}}, \qquad \xi = \frac{\vartheta \tilde{\mathscr{F}}^{-1/2} \check{\xi}}{\sqrt{12(1-\nu^2)}}, \qquad \eta = \frac{\vartheta \tilde{\mathscr{F}}^{1/2} \check{\eta}}{\sqrt{12(1-\nu^2)}}, \qquad \zeta = \frac{\vartheta \check{\zeta}}{\sqrt{12(1-\nu^2)}}. \tag{7.10}$$

(The $O(1)$ factors of $\sqrt{12(1-\nu^2)}$ have been introduced for convenience in the calculations below.) Substituting these expressions into the equilibrium equations (3.21)–(3.23), we obtain the following leading-order equations for the Ia bending layer:

$$\frac{\partial^4 \check{\xi}}{\partial \check{z}^4} - \frac{\partial^2 \check{\xi}}{\partial \check{z}^2} = 0, \tag{7.11}$$

$$\frac{\partial^2 \check{\eta}}{\partial \check{z}^2} = 0, \tag{7.12}$$

$$\frac{\partial^2 \check{\zeta}}{\partial \check{z}^2} = 0, \tag{7.13}$$

with errors of $O(\vartheta \tilde{\mathscr{F}}^{-1})$, $O(\vartheta \tilde{\mathscr{F}}^{-1}, \tilde{\mathscr{F}})$, and $O(\vartheta \tilde{\mathscr{F}}^{-1}, \tilde{\mathscr{F}})$, respectively.

By inspection, the general solution of (7.11)–(7.13) is

$$\check{\xi} = \check{A} \mathrm{e}^{-\check{z}} + \check{B} \mathrm{e}^{\check{z}} + \check{C}\check{z} + \check{D}, \tag{7.14}$$

$$\check{\eta} = \check{E}\check{z} + \check{F}, \tag{7.15}$$

$$\check{\zeta} = \check{G}\check{z} + \check{H}, \tag{7.16}$$

where $\check{A}$–$\check{H}$ are all arbitrary functions of τ.

7.3. *Boundary conditions and matching*

Applying the boundary conditions (2.11) at $z = 0$ to solution (7.14)–(7.16) in the Ia bending layer, and suppressing the exponential growth into the interior ($\check{z} \to \infty$), we obtain

$$\check{B} = \check{F} = \check{H} = 0, \qquad \check{A} = \check{C} = -\check{D}. \tag{7.17}$$

Hence the solution in the Ia bending layer simplifies to

$$\check{\xi} = \check{A}\left(e^{-\check{z}} - 1 + \check{z}\right), \tag{7.18}$$

$$\check{\eta} = \check{E}\check{z}, \tag{7.19}$$

$$\check{\zeta} = \check{G}\check{z}. \tag{7.20}$$

We now consider the solution (7.6)–(7.8) in the Ia inner shear layer. Suppressing the exponential growth into the interior ($\hat{z} \to \infty$), and ensuring decay of the displacements as $\hat{z} \to 0$ to match with the smaller scales in the bending layer, we must take $\hat{B} = 0$, $\hat{C} = \hat{D} = -\hat{A}$, and $\hat{F} = -\frac{\partial}{\partial \tau}\left((2 + \nu)\hat{A}/h\bar{b}\right)$. The solution (7.6)–(7.8) in the Ia inner shear layer solution then simplifies to

$$\hat{\xi} = \hat{A}\left(e^{-|\bar{B}|\hat{z}} - 1\right), \tag{7.21}$$

$$\hat{\eta} = \frac{\partial}{\partial \tau}\left[\frac{(2 + \nu)}{h\bar{B}}\hat{A}\left(e^{-|\bar{B}|\hat{z}} - 1\right) + \frac{\bar{B}}{2\nu h}\hat{A}\hat{z}^2\right] + \hat{E}\hat{z}, \tag{7.22}$$

$$\hat{\zeta} = \frac{\nu\hat{A}}{h}\left(e^{-|\bar{B}|\hat{z}} - 1 - \frac{\bar{B}}{\nu^2}\hat{z}\right), \tag{7.23}$$

$$\tilde{S} = \tilde{\mathscr{F}}\frac{12(1 - \nu)}{2h}\left[\frac{\partial}{\partial \tau}\left(\frac{2(1 + \nu)}{h}\hat{A}e^{-|\bar{B}|\hat{z}} - \frac{\nu\hat{A}}{h}\right) + \hat{E}\right]. \tag{7.24}$$

We now complete the matching between the bending layer solution (7.18)–(7.20) as $\check{z} \to \infty$ and the shear layer solution (7.21)–(7.23) as $\hat{z} \to 0$. Equating the linear behaviour of ξ, η and ζ in the matching region, we obtain

$$\check{A} = \bar{B}\hat{A}, \qquad \check{E} = (2 + \nu)\frac{\partial}{\partial \tau}\left(\frac{\hat{A}}{h}\right) + \hat{E}, \qquad \check{G} = -\frac{(1 - \nu^2)\bar{B}}{\nu h}\hat{A}, \tag{7.25}$$

since $\bar{B} < 0$. (Note that $\tilde{S}$ in (7.24) has not been used in this matching, but will be needed in the next matching below.)

Next, we match the solution (7.21)–(7.24) in the Ia inner shear layer as $\hat{z} \to \infty$ to the intermediate solution (5.2) and (5.5)–(5.7) as $z \to 0$. We find that

$$\hat{A} = -\frac{\nu h}{12(1 - \nu^2)\bar{B}}C_0, \qquad \hat{E} = \frac{1}{12(1 - \nu^2)}\left[A_1 - \frac{\partial}{\partial \tau}\left(\frac{\nu^2 C_0}{\bar{B}}\right)\right], \tag{7.26}$$

and

$$A_0 = D_0 = E_0 = 0; \tag{7.27}$$

while B_0, B_1 and C_1 are unconstrained at this order. (Observe that matching $\tilde{S}$ is necessary to obtain the equation for $\hat{E}$.)

Finally, we match the outer limit of the stresses (5.1)–(5.3) and displacements (5.5)–(5.7) in the intermediate solution as $z \to \infty$, with the inner limit of the corresponding outer-shear-layer solutions (B.4)–(B.6) and (B.7)–(B.9) as $\breve{z} \to 0$. First, we set $\mathscr{C} = \tilde{\mathscr{F}}^{1/2}$ to match the dominant behaviour between the layers (in particular, the z^0 terms in $\tilde{\Sigma}$). Then, completing the matching, we find that

$$A_0 = B_0 = 0, \tag{7.28}$$

$$C_0 = \sum_{n=1}^{\infty} \breve{B}_n Y_n(\tau), \tag{7.29}$$

$$A_1 = 2(1+\nu) \sum_{n=1}^{\infty} \frac{\breve{B}_n}{\mu_n} \frac{\partial}{\partial \tau} \left[\frac{1}{\bar{B}^2 h} \frac{\partial}{\partial \tau} \left(\frac{1}{h} \frac{\partial Y_n}{\partial \tau} \right) - Y_n(\tau) \right], \tag{7.30}$$

$$B_1 = -\sum_{n=1}^{\infty} \mu_n \breve{B}_n Y_n(\tau), \tag{7.31}$$

$$\breve{D}_n = \breve{E}_n = 0, \tag{7.32}$$

while C_1, D_0, and E_0 are unconstrained. Note that the expressions here for A_0 and B_0 are consistent with (5.4), as are those for A_1 and B_1 by virtue of the eigenvalue equation (B.1).

This concludes the matching. All the arbitrary constants/functions of integration have been determined in terms of the coefficients $\breve{B}_n$ from the outer shear layer, with the exception of C_1 that would require higher-order matching.

7.4. *Final matched solutions*

Combining the matched results above, the leading-order solutions in each layer are as follows. The solutions are written in terms of a single set of amplitudes $\breve{B}_n$ for the azimuthal modes $Y_n(\tau)$ in the outer shear layer. In any given problem, these amplitudes $\breve{B}_n$ would be determined by matching the outer shear layer to the bulk solution at $z = O(\ell)$.

In the outer shear layer $1 \ll z \ll \ell$ with $\breve{z} = z/\tilde{\mathscr{F}}^{-1/2}$ we have

$$\xi = \frac{\tilde{\mathscr{F}}^{-1/2}}{12(1-\nu^2)\bar{B}(\tau)} \sum_{n=1}^{\infty} \frac{\breve{B}_n}{\mu_n} \left[\frac{1}{\mu_n} \left(1 - e^{-\mu_n \breve{z}} \right) - \breve{z} \right] \left(\frac{Y_n'}{h} \right)', \tag{7.33}$$

$$\eta = \frac{\tilde{\mathscr{F}}^{-1/2}}{12(1-\nu^2)} \sum_{n=1}^{\infty} \frac{\breve{B}_n}{\mu_n} \left[\frac{1}{\mu_n} \left(1 - e^{-\mu_n \breve{z}} \right) - \breve{z} \right] Y_n'(\tau), \tag{7.34}$$

$$\zeta = \frac{1}{12(1-\nu^2)} \sum_{n=1}^{\infty} \frac{\breve{B}_n}{\mu_n} \left(1 - e^{-\mu_n \breve{z}} \right) Y_n(\tau). \tag{7.35}$$

In the intermediate region $\tilde{\mathscr{F}}^{1/2} \ll z \ll \tilde{\mathscr{F}}^{-1/2}$ we have

$$\xi = \frac{\tilde{\mathscr{F}}^{1/2}}{12(1-\nu^2)\bar{B}}\left[\nu h \sum_{n=1}^{\infty}\breve{B}_n Y_n - \frac{1}{2}\sum_{n=1}^{\infty}\breve{B}_n\left(\frac{Y_n'}{h}\right)' z^2\right], \tag{7.36}$$

$$\eta = \frac{\tilde{\mathscr{F}}^{1/2}}{12(1-\nu^2)}\left(-\frac{1}{2}\sum_{n=1}^{\infty}\breve{B}_n Y_n'\right)z^2, \tag{7.37}$$

$$\zeta = \frac{\tilde{\mathscr{F}}^{1/2}}{12(1-\nu^2)}\left(\sum_{n=1}^{\infty}\breve{B}_n Y_n\right)z. \tag{7.38}$$

In the Ia shear layer $\vartheta\tilde{\mathscr{F}}^{-1/2} \ll z \ll 1$ with $\hat{z}=z/\tilde{\mathscr{F}}^{1/2}$, we have

$$\xi = \frac{\tilde{\mathscr{F}}^{1/2}\nu h}{12(1-\nu^2)\bar{B}}\left(\sum_{n=1}^{\infty}\breve{B}_n Y_n\right)\left(1-e^{-|\bar{B}|\hat{z}}\right), \tag{7.39}$$

$$\eta = \frac{\tilde{\mathscr{F}}^{3/2}}{12(1-\nu^2)}\frac{\partial}{\partial\tau}\left[\left(\sum_{n=1}^{\infty}\breve{B}_n Y_n\right)\left(\frac{(2+\nu)\nu}{\bar{B}^2}\left(1-e^{-|\bar{B}|\hat{z}}\right)-\frac{1}{2}\hat{z}^2\right)\right.$$
$$\left.+\sum_{n=1}^{\infty}\breve{B}_n\left\{\frac{2(1+\nu)}{\mu_n\bar{B}^2 h}\frac{\partial}{\partial\tau}\left(\frac{1}{h}\frac{\partial Y_n}{\partial\tau}\right)-\left(\frac{\nu^2}{\bar{B}}+\frac{2(1+\nu)}{\mu_n}\right)Y_n\right\}\hat{z}\right], \tag{7.40}$$

$$\zeta = \frac{\tilde{\mathscr{F}}}{12(1-\nu^2)}\left(\sum_{n=1}^{\infty}\breve{B}_n Y_n\right)\left(\frac{\nu^2}{\bar{B}}\left(1-e^{-|\bar{B}|\hat{z}}\right)+\hat{z}\right). \tag{7.41}$$

In the Ia bending layer $z \ll \tilde{\mathscr{F}}^{1/2}$ with $\check{z}=z\sqrt{12(1-\nu^2)}/(\vartheta\tilde{\mathscr{F}}^{-1/2})$, we have

$$\xi = \frac{\vartheta\tilde{\mathscr{F}}^{-1/2}\nu h}{[12(1-\nu^2)]^{3/2}}\left(\sum_{n=1}^{\infty}\breve{B}_n Y_n\right)\left(1-\check{z}-e^{-\check{z}}\right), \tag{7.42}$$

$$\eta = \frac{\vartheta\tilde{\mathscr{F}}^{1/2}2(1+\nu)}{[12(1-\nu^2)]^{3/2}}\sum_{n=1}^{\infty}\breve{B}_n\left\{-\nu\left(\frac{Y_n}{\bar{B}}\right)'+\frac{1}{\mu_n}\left(\frac{1}{\bar{B}^2 h}\left(\frac{Y_n'}{h}\right)'-Y_n\right)'\right\}\check{z}, \tag{7.43}$$

$$\zeta = \frac{\vartheta}{12^{3/2}(1-\nu^2)^{1/2}}\left(\sum_{n=1}^{\infty}\breve{B}_n Y_n\right)\check{z}. \tag{7.44}$$

The order-of-magnitude of ξ, η and ζ in the different boundary layers, and the power-law behaviour between them is shown in Figure 4(a).

8. Regime Ib ($\tilde{\mathscr{F}} \ll \vartheta \ll 1$)

We now consider in detail the boundary layers that exist in Regime Ib, where $\tilde{\mathscr{F}} \ll \vartheta \ll 1$. The governing equations in each layer are derived and solved at leading order, and then the solutions are matched to give a full solution. In this regime, we have $\vartheta \gg \tilde{\mathscr{F}}$, which implies $\tilde{\mathscr{F}}^{-1/2} \gg \ell$. Hence, from the analysis in §4, we have a single bulk shear layer when $z \gg 1$, with width $O(\ell)$. From (4.2), we have
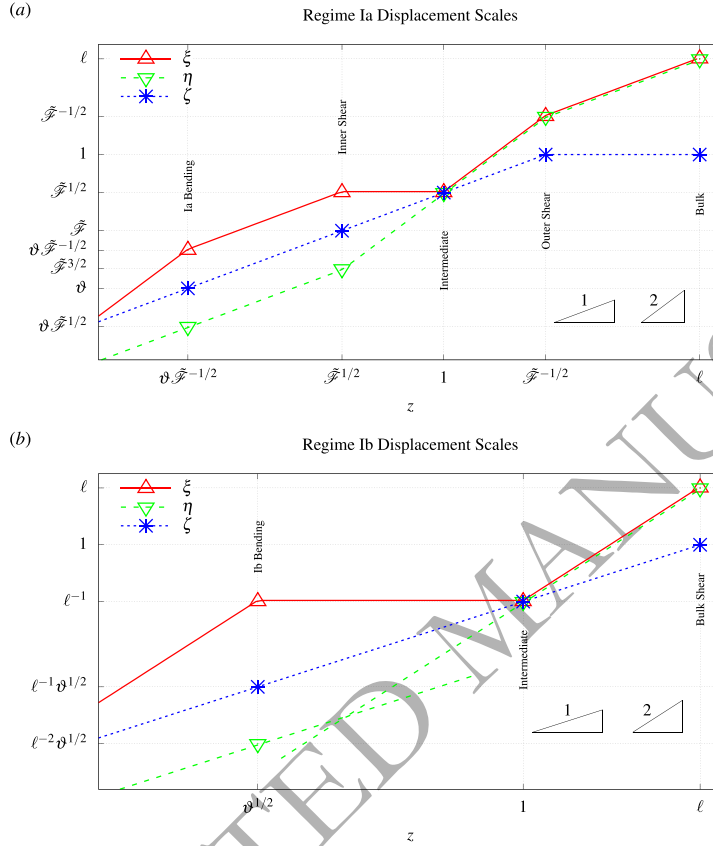
FIG. 4. The order-of-magnitude of the three displacement functions ξ, η and ζ in the different boundary layers, and the power-law behaviour (z^α for $\alpha = 0, 1, 2$) in the regions between them. The two intersecting dashed lines in (b) reflect a change in the asymptotic order of the z and z^2 terms in the expansion of η between the Ib Bending layer and the Intermediate region.

$\varepsilon = \vartheta^2 \ell^4 a^3 P/K$ and $\mathscr{P} = \ell^{-3}$. The intermediate region at $z = O(1)$ was considered in §5. Here we consider the expected layer for $z \ll 1$, as anticipated in §6.4, namely a Ib bending layer at $z = O(\vartheta^{1/2})$. We will then complete the matching between the various boundary layers.

8.1. *Ib bending layer $z = O(\vartheta^{1/2})$*

In the Ib bending layer, we expect a dominant balance between axial bending and the azimuthal hoop stress in the normal direction, with ξ is present at leading order in both of these terms (see §6.4). The scaling for ξ is set by the need to match to the behaviour $\xi = O(\ell^{-1})$ as $z \to 0$ from the intermediate region. We then take $\zeta \sim \delta\xi$ so that it can also contribute to the hoop stress. The scaling for η is determined by the need to match the shear stress $\tilde{S}$ with the intermediate region.[1]

---

[1] We have $\tilde{S} \sim \partial\eta/\partial z$ here, and it turns out this needs to match with the A_1 term in (5.2), which has a magnitude of $O(\mathscr{C}^2) = O(\ell^{-2})$. Hence $\eta \sim \vartheta^{1/2}\ell^{-2}$.

We therefore introduce $O(1)$ scaled variables $\{\mathring{z}, \mathring{\xi}, \mathring{\eta}, \mathring{\zeta}\}$ and write:

$$z = \vartheta^{1/2} \cdot \frac{\sqrt{2}}{\left[12(1-v^2)\right]^{1/4}} \cdot \mathring{z}, \qquad \xi = \ell^{-1} \cdot vh \cdot \mathring{\xi}, \tag{8.1}$$

$$\eta = \ell^{-2} \vartheta^{1/2} \cdot \frac{\sqrt{2}}{\left[12(1-v^2)\right]^{1/4}} \cdot \mathring{\eta}, \qquad \zeta = \ell^{-1} \vartheta^{1/2} \cdot \frac{\sqrt{2}\,v^2}{\left[12(1-v^2)\right]^{1/4}} \cdot \mathring{\zeta}. \tag{8.2}$$

(The $O(1)$ factors of $\sqrt{2}$, $12(1-v^2)$, v and h are introduced for convenience in the calculations that follow.) On substituting (8.1)–(8.2) into (3.21)–(3.23), we obtain the following leading-order equilibrium equations for the Ib bending layer:

$$(1-v^2)\frac{\partial^4 \mathring{\xi}}{\partial \mathring{z}^4} + 4\bar{B}^2 \mathring{\xi} - 4v^2 \bar{B}\frac{\partial \mathring{\zeta}}{\partial \mathring{z}} = 0, \tag{8.3}$$

$$\frac{\partial^2 \mathring{\eta}}{\partial \mathring{z}^2} = 0, \tag{8.4}$$

$$\frac{\partial^2 \mathring{\zeta}}{\partial \mathring{z}^2} - \bar{B}\frac{\partial \mathring{\xi}}{\partial \mathring{z}} = 0, \tag{8.5}$$

with errors of $O(\ell^{-2}, \bar{\mathscr{F}}\vartheta^{-1})$, $O(\ell\vartheta^{1/2}, \bar{\mathscr{F}})$ and $O(\ell^{-1}\vartheta^{1/2}, \bar{\mathscr{F}})$ respectively.

We eliminate $\mathring{\xi}$ between (8.3) and (8.5) by differentiating (8.3) with respect to $\mathring{z}$, and then substituting for $\partial \mathring{\xi}/\partial \mathring{z}$ using (8.5). We obtain

$$\frac{\partial^6 \mathring{\zeta}}{\partial \mathring{z}^6} + 4\bar{B}^2 \frac{\partial^2 \mathring{\zeta}}{\partial \mathring{z}^2} = 0. \tag{8.6}$$

The general solution of this equation is

$$\begin{aligned}
\mathring{\zeta} &= \left(\mathring{A}\cos(|\bar{B}|^{1/2}\mathring{z}) + \mathring{B}\sin(|\bar{B}|^{1/2}\mathring{z})\right)e^{-|\bar{B}|^{1/2}\mathring{z}} \\
&\quad + \left(\mathring{C}\cos(|\bar{B}|^{1/2}\mathring{z}) + \mathring{D}\sin(|\bar{B}|^{1/2}\mathring{z})\right)e^{|\bar{B}|^{1/2}\mathring{z}} + \mathring{E} + \mathring{F}\mathring{z},
\end{aligned} \tag{8.7}$$

where $\mathring{A}$–$\mathring{F}$ are arbitrary functions of τ.

We now re-arrange (8.3) for $\mathring{\xi}$, and eliminate $\partial^4 \mathring{\xi}/\partial \mathring{z}^4$ using (8.5). Noting that $\bar{B} < 0$, this gives

$$\mathring{\xi} = \frac{(1-v^2)}{4|\bar{B}|^3}\frac{\partial^5 \mathring{\zeta}}{\partial \mathring{z}^5} - \frac{v^2}{|\bar{B}|}\frac{\partial \mathring{\zeta}}{\partial \mathring{z}}, \tag{8.8}$$

from which we obtain

$$\begin{aligned}
\mathring{\xi} &= |\bar{B}|^{-1/2}\left((\mathring{A}-\mathring{B})\cos(|\bar{B}|^{1/2}\mathring{z}) + (\mathring{A}+\mathring{B})\sin(|\bar{B}|^{1/2}\mathring{z})\right)e^{-|\bar{B}|^{1/2}\mathring{z}} \\
&\quad + |\bar{B}|^{-1/2}\left(-(\mathring{C}+\mathring{D})\cos(|\bar{B}|^{1/2}\mathring{z}) + (\mathring{C}-\mathring{D})\sin(|\bar{B}|^{1/2}\mathring{z})\right)e^{|\bar{B}|^{1/2}\mathring{z}} - \frac{v^2}{|\bar{B}|}\mathring{F}.
\end{aligned} \tag{8.9}$$

The general solution of (8.4) for $\mathring{\eta}$ is

$$\mathring{\eta} = \mathring{G}\mathring{z} + \mathring{H}, \tag{8.10}$$

where $\mathring{G}$ and $\mathring{H}$ are two more arbitrary functions of τ.

8.2. *Boundary conditions and matching*

Applying the boundary conditions (2.11) at $z = 0$ to the Ib bending-layer solution (8.7), (8.9) and (8.10), and suppressing exponential growth into the interior ($\mathring{z} \to \infty$), we find that we must take

$$\mathring{B} = \mathring{C} = \mathring{D} = \mathring{H} = 0, \qquad \mathring{E} = -\mathring{A}, \qquad \mathring{F} = |\bar{B}|^{1/2}\mathring{A}/\nu^2. \tag{8.11}$$

The solution in the bending layer then simplifies to

$$\mathring{\xi} = -\mathring{A}\,|\bar{B}|^{-1/2}\left[1 - \left(\cos(|\bar{B}|^{1/2}\mathring{z}) + \sin(|\bar{B}|^{1/2}\mathring{z})\right)\mathrm{e}^{-|\bar{B}|^{1/2}\mathring{z}}\right], \tag{8.12}$$

$$\mathring{\eta} = \mathring{G}\mathring{z}, \tag{8.13}$$

$$\mathring{\zeta} = -\mathring{A}\left[1 - \nu^{-2}|\bar{B}|^{1/2}\mathring{z} - \cos(|\bar{B}|^{1/2}\mathring{z})\,\mathrm{e}^{-|\bar{B}|^{1/2}\mathring{z}}\right]. \tag{8.14}$$

From (3.11), the shear stress in the bending boundary layer (which we need for further matching) is then given by

$$\tilde{S} = \ell^{-2}\frac{12(1-\nu)}{2h}\frac{\partial\mathring{\eta}}{\partial\mathring{z}} + O\left(\ell^{-1}\vartheta^{1/2}\right) \sim \ell^{-2}\frac{12(1-\nu)}{2h}\mathring{G}. \tag{8.15}$$

Matching the bending-layer solution (8.12)–(8.15) as $\mathring{z} \to \infty$ with the intermediate solution (5.2) and (5.5)–(5.7) as $z \to 0$, we find that

$$A_0 = D_0 = E_0 = 0, \qquad C_0 = 12(1-\nu^2)|\bar{B}|^{1/2}\mathring{A}, \qquad A_1 = 12(1-\nu^2)\mathring{G}. \tag{8.16}$$

The other coefficients are unconstrained at leading order.

Finally, we match the outer limit of the stresses (5.1)–(5.3) and displacements (5.5)–(5.7) in the intermediate solution as $z \to \infty$, with the inner limit of the corresponding solutions (C.13), (C.16), (C.11), and (C.17)–(C.19) in the Ib bulk shear layer as $\hat{z} \to 0$. The latter involves a set of amplitude functions $q_n(\hat{z})$ for the azimuthal modes $Y_n(\tau)$. The $Y_n(\tau)$ are fully determined, while the $q_n(\hat{z})$ must satisfy the ordinary differential equations (C.10) and (C.15). The matching provides boundary conditions on the $q_n(\hat{z})$, and also expressions for the unknown amplitudes in the intermediate solution in terms of higher derivatives of q_n at $\hat{z} = 0$. First, we note that $\mathscr{P} = \ell^{-3}$ from (C.20), and set $\mathscr{C} = \ell^{-1}$ to match the dominant behaviours between the layers (in particular, the z^0 terms in $\tilde{\Sigma}$). Then, completing the matching, we find that

$$q_0(0) = 0, \qquad q_n(0) = q_n'(0) = 0 \quad (n = 1, 2, 3, \ldots), \tag{8.17}$$

together with

$$A_0(\tau) = 0, \qquad B_0(\tau) = 0, \qquad C_0(\tau) = q_0'(0) + \sum_{n=1}^{\infty} q_n''(0)\,Y_n(\tau), \tag{8.18}$$

$$A_1(\tau) = -2(1+\nu)\sum_{n=1}^{\infty}\frac{q_n'''(0)}{\mu_n^2}\frac{\partial}{\partial\tau}\left(\frac{1}{\bar{B}^2 h}\frac{\partial}{\partial\tau}\frac{1}{h}\frac{\partial Y_n}{\partial\tau} - Y_n\right), \qquad B_1(\tau) = \sum_{n=1}^{\infty}q_n'''(0)\,Y_n(\tau). \tag{8.19}$$

The remaining functions D_0, E_0 and C_1 in the intermediate solution are unconstrained by this matching at leading order. Note that the expressions here for A_0 and B_0 are consistent with (5.4), as are those for A_1 and B_1 by virtue of the eigenvalue equation (B.1).

An analysis of the boundary layers and matching near the $z = \ell$ end of the tube will result in equivalent conditions to (8.17)–(8.19) involving the coefficients for the boundary layers at the other end of the tube, and with $\hat{z} = 0$ replaced by $\hat{z} = 1$. Since $q_0''(\hat{z}) = 0$, the conditions $q_0(0) = q_0(1) = 0$, mean that $q_0(\hat{z}) \equiv 0$ for all $\hat{z}$.

8.3. *Final matched solution*

Combining the matched results above, the leading-order solutions in each layer are as follows. The solutions are written in terms of a single set of functions $q_n(\hat{z})$ for $n = 1, 2, 3\ldots$, which give the amplitudes of the azimuthal modes $Y_n(\tau)$ in the bulk shear layer. These functions satisfy

$$q_n'''' - \left(\ell^2 \tilde{\mathscr{F}} \mu_n^2\right) q_n'' = -Q_n\,, \tag{8.20}$$

subject to

$$q_n(0) = q_n'(0) = 0\,, \qquad q_n(1) = q_n'(1) = 0\,, \tag{8.21}$$

where the Q_n (which may be $\hat{z}$-dependent) are defined in terms of the pressure forcing $\tilde{p}$ by (C.8).

In the bulk shear layer $1 \ll z$ and $1 \ll \ell - z$ with $\hat{z} = z/\ell$ we have

$$\xi \sim -\frac{\ell}{12(1-\nu^2)\bar{B}} \sum_{n=1}^{\infty} \frac{\partial}{\partial \tau} \left(\frac{1}{h} \frac{\partial Y_n}{\partial \tau}\right) q_n(\hat{z})\,, \tag{8.22}$$

$$\eta \sim -\frac{\ell}{12(1-\nu^2)} \sum_{n=1}^{\infty} \frac{\partial Y_n}{\partial \tau} q_n(\hat{z})\,, \tag{8.23}$$

$$\zeta \sim \frac{1}{12(1-\nu^2)} \sum_{n=1}^{\infty} Y_n(\tau) q_n'(\hat{z})\,. \tag{8.24}$$

In the intermediate region $\vartheta^{1/2} \ll z \ll \tilde{\mathscr{F}}^{-1/2}$ we have

$$\xi = \frac{\ell^{-1}}{12(1-\nu^2)\bar{B}} \left[\nu h \sum_{n=1}^{\infty} q_n''(0) Y_n - \frac{1}{2} \sum_{n=1}^{\infty} q_n''(0) \frac{\partial}{\partial \tau} \left(\frac{1}{h} \frac{\partial Y_n}{\partial \tau}\right) z^2\right]\,, \tag{8.25}$$

$$\eta = -\frac{\ell^{-1}}{12(1-\nu^2)} \left(\frac{1}{2} \sum_{n=1}^{\infty} q_n''(0) \frac{\partial Y_n}{\partial \tau}\right) z^2\,, \tag{8.26}$$

$$\zeta = \frac{\ell^{-1}}{12(1-\nu^2)} \left(\sum_{n=1}^{\infty} q_n''(0) Y_n\right) z\,. \tag{8.27}$$

In the Ib bending layer $z \ll 1$ with $\mathring{z} = z\left[12(1-\nu^2)\right]^{1/4}/(\sqrt{2}\vartheta^{1/2})$, we have

$$\xi = -\frac{\ell^{-1}\nu h}{12(1-\nu^2)|\bar{B}|} \sum_{n=1}^{\infty} q_n''(0) Y_n(\tau) \left[1 - \left(\cos(|\bar{B}|^{1/2}\mathring{z}) + \sin(|\bar{B}|^{1/2}\mathring{z})\right) e^{-|\bar{B}|^{1/2}\mathring{z}}\right]\,, \tag{8.28}$$

$$\eta = -\frac{\ell^{-2}\vartheta^{1/2} 2\sqrt{2}(1+\nu)}{[12(1-\nu^2)]^{5/4}} \sum_{n=1}^{\infty} \frac{q_n'''(0)}{\mu_n^2} \frac{\partial}{\partial \tau} \left(\frac{1}{\bar{B}^2 h} \frac{\partial}{\partial \tau} \frac{1}{h} \frac{\partial Y_n}{\partial \tau} - Y_n\right) \mathring{z}\,, \tag{8.29}$$

$$\zeta = \frac{\ell^{-1}\vartheta^{1/2}\sqrt{2}}{[12(1-\nu^2)]^{5/4}} \sum_{n=1}^{\infty} q_n''(0) Y_n(\tau) \left[-\frac{\nu^2}{|\bar{B}|^{1/2}} \left(1 - \cos(|\bar{B}|^{1/2}\mathring{z}) e^{-|\bar{B}|^{1/2}\mathring{z}}\right) + \mathring{z}\right] \tag{8.30}$$

The orders-of-magnitude of ξ, η and ζ in the different boundary layers, and the power law behaviour between them is shown in Figure 4(*b*).

9. Regime Iab ($\tilde{\mathscr{F}} \sim \vartheta \ll 1$)

When $\tilde{\mathscr{F}}$ and ϑ are both small, but comparable in size, we find ourselves in an intermediate regime between Regime Ia and Regime Ib. In this case, using $\tilde{\mathscr{F}} \sim \ell^2 \vartheta^2$ from (2.2), we have

$$\vartheta \sim \tilde{\mathscr{F}} \sim \tilde{\mathscr{F}}^{1/2} \cdot \ell \vartheta \quad \Rightarrow \quad \ell \tilde{\mathscr{F}}^{1/2} = O(1). \tag{9.1}$$

With $\vartheta \sim \tilde{\mathscr{F}}$, the three distinguished limits depicted in Figure 3 all coincide at $\delta = O(\tilde{\mathscr{F}}^{1/2})$. Hence there is just one inner boundary layer for $z \ll 1$, which involves all three effects (azimuthal hoop stress, pre-stress/curvature, and axial bending). With $\ell \sim \tilde{\mathscr{F}}^{-1/2}$, we have a single single bulk outer layer for $z \gg 1$, which combines the pressure forcing and in-plane shear effects. The behaviours in these two layers must be matched through the intermediate region $z = O(1)$. The boundary layer structure is thus the same as in Regime Ib, though additional physical effects are present in each layer here.

Regime Iab can be analysed in a similar manner to the other two Regimes, though we omit the full details for brevity. If we write $\vartheta = \lambda^2 \tilde{\mathscr{F}}$, where $\lambda = O(1)$, and use the previous variables $\hat{\xi} = \xi/\tilde{\mathscr{F}}^{1/2}$ and $\hat{z} = z/\tilde{\mathscr{F}}^{1/2}$, then the differential equation governing the leading-order normal displacements in the inner boundary layer is

$$\frac{\lambda^4}{12(1-\nu^2)} \frac{\partial^5 \hat{\xi}}{\partial \hat{z}^5} - \frac{\partial^3 \hat{\xi}}{\partial \hat{z}^3} + \bar{B}^2 \frac{\partial \hat{\xi}}{\partial \hat{z}} = 0. \tag{9.2}$$

In the (singular) limit $\lambda \to 0$, we recover the Ia shear layer of §7.1, with the Ia bending layer of §7.2 as a boundary layer within it. In the limit $\lambda \to \infty$, a re-scaling will recover the Ib bending layer of §8.1.

The outer bulk shear layer in this regime is considered in Appendix C. Since $\ell^2 \tilde{\mathscr{F}} = O(1)$, that term must be retained in the equation (C.10) for the $q_n(\hat{z})$. In the limit $\lambda \to \infty$, the Regime Ib bulk shear trivially layer is recovered. In the limit $\lambda \to 0$ a boundary-layer analysis would be required to recover the separate bulk and outer shear layers of Regime Ia.

In Regime Iab, the boundary-layer structure and the order-of-magnitude of ξ, η and ζ in the different boundary layers is the same as in Regime Ib, as shown in Figure 4(*b*), with the additional relations $\ell \sim \tilde{\mathscr{F}}^{-1/2}$ and $\vartheta \sim \tilde{\mathscr{F}}$.

10. Comparison

To assess the validity of the matched asymptotic solutions derived here, we compare them with solutions to the full problem (3.21)–(3.23). We consider the limiting case of a circular initial cross-section, since in this case, exact solutions can be obtained to (3.21)–(3.23).

We consider an initially circular tube, corresponding to $\sigma_0 = \infty$, with deformations induced by the non-azimuthally-uniform transmural pressure $\tilde{p} = -\cos 2\tau$. The details of the exact solutions can be found in Appendix D, while the corresponding calculations for the asymptotic solutions in each regime can be found in Appendices E and F. In all cases, the solutions for $\xi(\tau,z)$ and $\zeta(\tau,z)$ are proportional to $\cos 2\tau$, while the solutions for $\eta(\tau,z)$ are proportional to $\sin 2\tau$.

An axially uniform pressure has been used for comparison to simplify the computation of the exact solution. The asymptotic theory developed here is also valid with non-axially uniform transmural pressures. But since the boundary-layer systems contain no direct forcing from the pressure, and are forced only by matching to the limiting form of the bulk solution as the boundary layers are approached, the comparison with an axially uniform pressure should be sufficient to validate the asymptotic theory.

For Regime Ia, graphs comparing the asymptotic and exact solutions in each layer can be found in Figures 5 and **??**. (To avoid cluttering the figures, we just show the asymptotic solution corresponding

to the layer being depicted in each plot, rather than a composite solution. Thus in figure 5*a* for the bulk, the asymptotic solutions do not show boundary-layer behaviour.) For Regime Ib, similar graphs comparing the asymptotic and exact solutions can be found in Figure 7. In each case, two different exact solutions are shown with different parameter values, to show the effect of being further from, and closer to, the asymptotic limit. The exact solutions from the closer sets of parameters (dotted lines) show excellent agreement with the asymptotic results (continuous lines), and the graphs are almost indistinguishable. The exact solutions that are further from the asymptotic limit (dot-dashed lines) show noticeable discrepancies on many of the graphs.
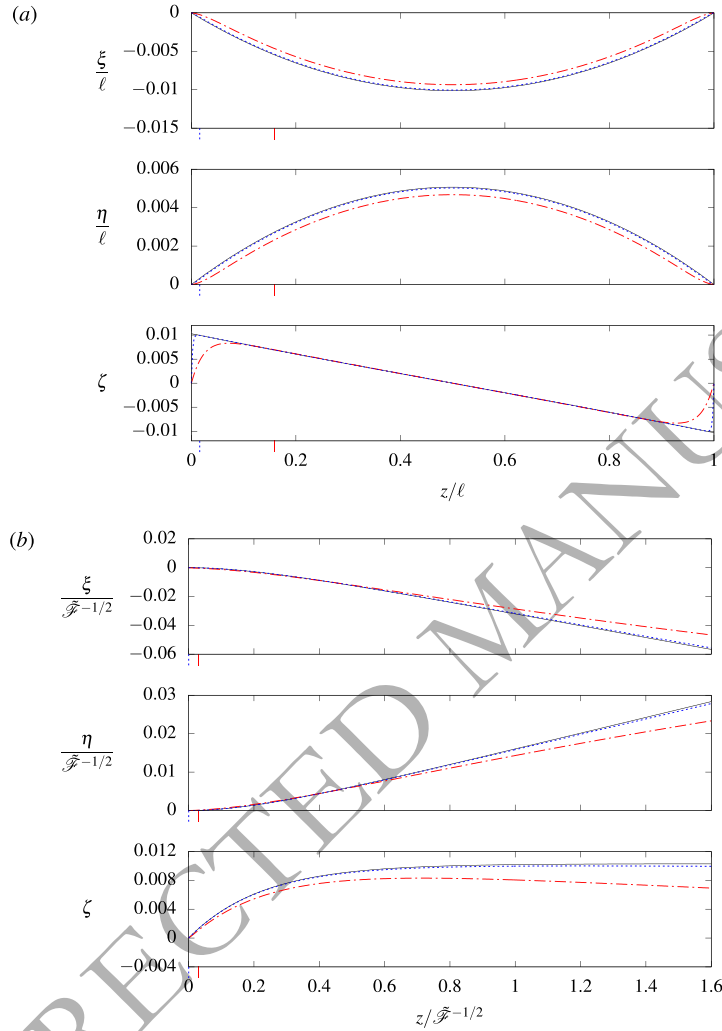
FIG. 5. Comparison of the asymptotic and exact solutions for Regime Ia, in (*a*) the bulk and (*b*) outer shear layer, as functions of the axial coordinate z. We consider the circular limit $\sigma_0 = \infty$ with $\nu = 0.49$ and transmural pressure $\tilde{p} = -\cos 2\tau$. For the normal and axial displacements ξ and ζ, we plot the coefficient of $\cos 2\tau$ in the solutions; for the azimuthal displacement, we plot the the coefficient of $\sin 2\tau$. In each case, the continuous line is the asymptotic solution for the layer from §7.4 or Appendix E, while the dot-dashed and dotted lines are exact solutions with $(\ell, \tilde{\mathscr{F}}, \vartheta) = (10^2, 10^{-2}, 10^{-3})$ and $(\ell, \tilde{\mathscr{F}}, \vartheta) = (10^4, 10^{-4}, 10^{-6})$ respectively, from Appendix D. The short vertical lines of the same style below the abscissa in (*a*) show the axial extent of the graphs in (*b*), and those in (*b*) show the axial extent in Figure **??**(*a*).

11. Discussion and conclusions

This paper provides the answer to the question of how solutions to a second-order (in the axial coordinate) tube-law used to describe fluid–structure-interaction problems should be adjusted to cope with the full set of clamped boundary conditions at the tube end in a particular region of parameter space.
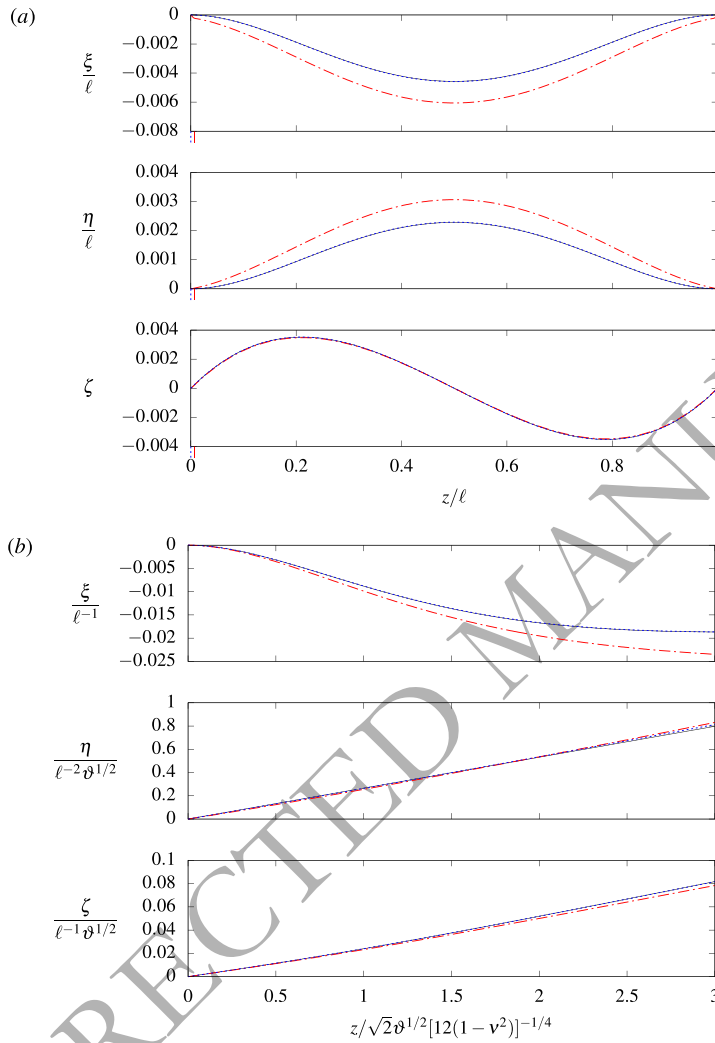
FIG. 7. Comparison of the asymptotic and exact solutions for Regime Ib, in (*a*) the bulk shear layer and (*b*) the bending layer, as functions of the axial coordinate z. We consider the circular limit $\sigma_0 = \infty$ with $\nu = 0.49$ and transmural pressure $\tilde{p} = -\cos 2\tau$. For the normal and axial displacements ξ and ζ, we plot the coefficient of $\cos 2\tau$ in the solutions; for the azimuthal displacement, we plot the the coefficient of $\sin 2\tau$. In each case, the continuous line is the asymptotic solution for the layer from §8.3 or Appendix F, while the dot-dashed and dotted lines are exact solutions with $(\ell, \tilde{\mathscr{F}}, \vartheta) = (10, 10^{-4}, 10^{-3})$ and $(\ell, \tilde{\mathscr{F}}, \vartheta) = (10^2, 10^{-8}, 10^{-6})$ respectively from Appendix D. The short vertical lines of the same style below the abscissa in (*a*) show the axial extent of the corresponding graphs in (*b*).

The initially elliptical elastic-walled tube considered here has circumference $2\pi a$ and length L, and is subject to an axial tension F. The tube wall has thickness d, Poisson ratio is ν, and bending stiffness K. An applied transmural pressure p causes deformations of the tube wall with normal amplitude e.

The key dimensionless parameters in the problem are: the dimensionless thickness of the tube wall, $\vartheta = d/a$; the dimensionless length of the tube, $\ell = L/a$; a scaled axial tension,

$\tilde{\mathscr{F}} = d^2 F / [2\pi a K (1 - v^2)]$; and the dimensionless deformation amplitude, $\varepsilon = e/a$. The problem is first linearised for $\varepsilon \ll 1$. We have then derived leading-order matched asymptotic solutions for the boundary-layer structure when $\ell^{-1}, \vartheta, \tilde{\mathscr{F}} \ll 1$, and showed that there are three distinct parameter regimes. In each regime, the axial thicknesses of the different boundary layers are described in terms of the dimensionless axial coordinate z, which is scaled on the cross-sectional length scale a. We therefore have that $z = 1$ corresponds to a length that is comparable with the width of the tube, while $z = \ell$ is the length of the tube.

In Regime Ia ($\vartheta \ll \tilde{\mathscr{F}} \ll 1$) there are three boundary layers: a bending layer with $z = O(\vartheta \tilde{\mathscr{F}}^{-1/2})$, an inner shear layer with $z = O(\tilde{\mathscr{F}}^{1/2})$, and outer shear layer with $z = O(\tilde{\mathscr{F}}^{-1/2})$. These are matched to each other and to the bulk solution with $z = O(\ell)$. The bending layer arises as a result of a balance between axial bending and axial pre-stress/curvature effects. The inner shear layer arises as a result of a balance between azimuthal hoop stress and axial pre-stress/curvature effects, with axial stress and shear stress also present at leading order. The outer shear layer arises as a result of a balance between axial stress and axial pre-stress/curvature effects, with shear stress and azimuthal hoop stress also present at leading order. In the bulk, the applied transmural pressure is balanced by a combination of azimuthal bending and axial pre-stress/curvature effects, with shear stress and azimuthal hoop stress also present at leading order.

In Regime Ib ($\tilde{\mathscr{F}} \ll \vartheta \ll 1$) there is only one boundary layer: a bending layer with $z = O(\vartheta^{1/2})$. This is matched to a bulk solution with $z = O(\ell)$. The bending layer arises as a result of a balance between axial bending and azimuthal hoop stress, with axial press-stress/curvature effects and axial stress also present at leading order. The leading-order balances in the bulk involve the applied transmural pressure and all three in-plane stresses.

In Regime Iab ($\vartheta \sim \tilde{\mathscr{F}} \ll 1$) the structure is as in Regime Ib, but with additional physical effects present in the boundary layer and bulk solutions. Both layers also contain axial pre-stress/curvature effects, in addition to the physical effects present in Regime Ib.

Since we are considering a linearised system, the magnitude P of the forcing from the transmural pressure affects neither the axial thicknesses nor the structure of the boundary layers. It only affects the amplitude of the deformations, through the dimensionless amplitude ε, as given in (2.3). The pressure scale just needs to be small enough so that $\varepsilon \ll 1$ holds. Moreover, as the boundary layers are only forced through the matching with the bulk solutions, the precise form of the transmural pressure (i.e. any z and τ dependence) also has no effect on the thicknesses and structure of the boundary layers. It can however affect the relative amplitudes of different azimuthal modes in the layers, through the coefficients $\check{B}_n$ in Regime Ia, and q_n'' and q_n''' in Regimes Ib and Iab.

The asymptotic solutions in Regimes Ia and Ib are shown in Figures 5–7, where they are seen to be in excellent agreement with full semi-analytic solutions for representative parameter values.

At leading order, the Ia shear layer here is the same as the inner shear layer that was found by Whittaker (2015) for the case where axial bending was ignored and only pinned boundary condition was imposed at $z = 0$. (A stress-variable formulation was used to derive it there, as opposed to the displacement formulation used here.) Corrections at the next order will alter the boundary layer slightly.

In the regimes considered here, the new bending boundary layers are passive, and have no leading-order effect on the interior solutions. (The outer shear layer can have an effect, as discussed in Whittaker (2015).)

The boundary layers described here were first considered in the PhD Thesis of Walters (2016). A slightly different approach was used to derive them in Regimes Ia and Ib, but here we prefer a common approach to both regimes. The results for the boundary layers are the same. However, Walters (2016)

did not realise the need to change the $z \gg 1$ behaviour in Regime Ib. It is possible to consider the solutions here as the first terms of an expansion in powers of ϑ and $\tilde{\mathscr{F}}$. Some of the first few correction terms can be found in Walters (2016).

We have not considered the regime in which $\tilde{\mathscr{F}} \geq O(1)$ in this paper. In this case, based on Kirchhoff–Love shell theory, the bending boundary layer would be predicted to be comparable to or narrower than the wall thickness. This means shell theory is no longer appropriate to describe the boundary layer. Initial work on the regime where $\tilde{\mathscr{F}} \gg 1$ can be found in Walters (2016).

A. Tensor evaluation

In this Appendix, we perform the calculations to evaluate the bending and stress tensors in terms of the displacement functions, in order to obtain the equilibrium equations in §3.

A.1. *Coordinates and strain*

If the wall centre-surface is given by $r(x^1, x^2)$ in terms of material coordinates x^1 and x^2, we can define basis vectors in the usual way by

$$a_\alpha = \frac{\partial r}{\partial x^\alpha} \quad \text{for} \quad \alpha \in 1, 2; \qquad a_3 = \frac{a_1 \times a_2}{|a_1 \times a_2|}. \tag{A.1}$$

Then the metric and curvature tensors are given by

$$a_{\alpha\beta} = a_\alpha \cdot a_\beta, \qquad b_{\alpha\beta} = a_3 \cdot \frac{\partial a_\alpha}{\partial x^\beta}. \tag{A.2}$$

The deformation of the wall material is characterised by in-plane strain and bending strain tensors, which we define as

$$\gamma_{\alpha\beta} = \frac{1}{2}\left(a_{\alpha\beta} - \bar{a}_{\alpha\beta}\right), \qquad \kappa_{\alpha\beta} = -b_{\alpha\beta} + \bar{b}_{\alpha\beta} + 2\bar{b}_\alpha^\delta \gamma_{\delta\beta}, \tag{A.3}$$

where over-bars denote the values of quantities in the undeformed configuration.

A.2. *Constitutive laws*

Linear constitutive laws relate the stress and stress moment resultants $N^{\alpha\beta}$ and $M^{\alpha\beta}$ to the strains $\gamma_{\alpha\beta}$ and $\kappa_{\alpha\beta}$ as follows (Flügge, 1972, §9.4):[2]

$$
\begin{aligned}
N^{\alpha\beta} &= \delta_2^\alpha \delta_2^\beta \frac{F}{2\pi a} + D\left[(1-\nu)\gamma^{\alpha\beta} + \nu\gamma_\lambda^\lambda a^{\alpha\beta}\right] \\
&\quad + K\left\{ \frac{(1-\nu)}{2}\left[2a^{\beta\delta}b^{\alpha\gamma} + a^{\beta\gamma}b^{\alpha\gamma} + a^{\alpha\delta}b^{\beta\gamma} - b_\lambda^\lambda(a^{\alpha\delta}a^{\beta\gamma} + a^{\alpha\gamma}a^{\beta\delta})\right] \right. \\
&\quad \left. + \nu\left[a^{\alpha\beta}b^{\gamma\delta} + a^{\gamma\delta}b^{\alpha\beta} - a^{\alpha\beta}a^{\gamma\delta}b_\lambda^\lambda\right] \right\} \kappa_{\gamma\delta},
\end{aligned} \tag{A.4}
$$

$$
\begin{aligned}
M^{\alpha\beta} &= K\left[-(1-\nu)(b_\gamma^\alpha\gamma^{\gamma\beta} - b_\lambda^\lambda\gamma^{\alpha\beta}) - \nu(b^{\alpha\beta} - b_\lambda^\lambda a^{\alpha\beta})\gamma_\mu^\mu \right. \\
&\quad \left. + \tfrac{1}{2}(1-\nu)(\kappa^{\alpha\beta} + \kappa^{\beta\alpha}) + \nu a^{\alpha\beta}\kappa_\lambda^\lambda \right],
\end{aligned} \tag{A.5}
$$

where δ_α^β is the Kronecker delta, ν is the Poisson ratio, and the extensional stiffness D is related to the bending stiffness K by

$$
D = \frac{12K}{a^2\vartheta^2}. \tag{A.6}
$$

The constitutive laws (A.4) and (A.5) arise from inserting the plane-stress form of Hooke's law into the definitions of $N^{\alpha\beta}$ and $M^{\alpha\beta}$, rewriting the resulting equations in terms of $\gamma_{\alpha\beta}$ and $\kappa_{\alpha\beta}$, and neglecting some higher-order terms in ϑ.

A.3. *Relation between the (x^1, x^2) and (τ, z) coordinates*

Our dimensionless coordinates τ and z are defined so that $\mathrm{d}x^1 = ah\,\mathrm{d}\tau$ and $\mathrm{d}x^2 = a\,\mathrm{d}z$. Hence

$$
\frac{\partial}{\partial x^1} = \frac{1}{ah}\frac{\partial}{\partial\tau}, \qquad \frac{\partial}{\partial x^2} = \frac{1}{a}\frac{\partial}{\partial z}. \tag{A.7}
$$

With the definitions of the unit vectors in (2.7), we then have

$$
\frac{\partial\hat{\imath}}{\partial\tau} = \bar{B}h\hat{n}, \qquad \frac{\partial\hat{n}}{\partial\tau} = -\bar{B}h\hat{\imath}, \qquad \frac{\partial\hat{z}}{\partial\tau} = 0. \tag{A.8}
$$

The corresponding partial derivatives with respect to z are all zero.

---

[2] Some signs in (A.2) differ from those in Flügge (1972). This is due to our opposing sign conventions on $\kappa_{\alpha\beta}$ and $M^{\alpha\beta}$, and later because of a sign error on the $(\kappa_{\alpha\beta} + \kappa_{\beta\alpha})$ term in Flügge's expression for $M^{\alpha\beta}$.

A.4. *Basis vectors*

The basis vectors a_i are computed from the definitions (A.1) using the expression for the position vector r in (2.9). The results are the same as in Whittaker (2015):

$$a_1 = \hat{\imath} + \frac{\varepsilon}{\ell h}\left[\left(-\xi\bar{B} + \frac{\partial}{\partial\tau}\left(\frac{\eta}{h}\right)\right)\hat{\imath} + \left(\eta\bar{B} + \frac{\partial}{\partial\tau}\left(\frac{\xi}{h}\right)\right)\hat{n}\right] + \frac{\varepsilon}{\ell h}\left[\frac{\partial\zeta}{\partial\tau}\hat{z}\right], \tag{A.9}$$

$$a_2 = \hat{z} + \frac{\varepsilon}{\ell}\left[\frac{1}{h}\frac{\partial\xi}{\partial z}\hat{n} + \frac{1}{h}\frac{\partial\eta}{\partial z}\hat{\imath} + \frac{\partial\zeta}{\partial z}\hat{z}\right], \tag{A.10}$$

$$a_3 = \hat{n} - \frac{\varepsilon}{\ell h}\left[\left(\eta\bar{B} + \frac{\partial}{\partial\tau}\left(\frac{\xi}{h}\right)\right)\hat{\imath} + \frac{\partial\xi}{\partial z}\hat{z}\right] + O\left(\frac{\varepsilon^2}{\ell^2}\right). \tag{A.11}$$

A.5. *Components of $b_{\alpha\beta}$, $\gamma_{\alpha\beta}$ and $\kappa_{\alpha\beta}$*

The following components were not all evaluated explicitly in Whittaker (2015), but are needed here for consideration of the bending layers.

From the expression (A.2) for the curvature tensor $b_{\alpha\beta}$, we obtain

$$\begin{aligned}
b_{11} &= a_3 \cdot \frac{1}{ah}\frac{\partial a_1}{\partial\tau} \\
&= \frac{\bar{B}}{a} + \frac{\varepsilon}{a\ell h}\left[\bar{B}\left(-\xi\bar{B} + \frac{\partial}{\partial\tau}\left(\frac{\eta}{\tau}\right)\right) + \frac{\partial}{\partial\tau}\left(\frac{\eta\bar{B}}{h} + \frac{1}{h}\frac{\partial}{\partial\tau}\left(\frac{\xi}{h}\right)\right)\right] + O\left(\frac{1}{a}\frac{\varepsilon^2}{\ell^2}\right),
\end{aligned} \tag{A.12}$$

$$b_{22} = a_3 \cdot \frac{1}{a}\frac{\partial a_2}{\partial z} = \frac{\varepsilon}{a\ell h}\frac{\partial^2\xi}{\partial z^2} + O\left(\frac{1}{a}\frac{\varepsilon^2}{\ell^2}\right). \tag{A.13}$$

$$b_{12} = b_{21} = a_3 \cdot \frac{1}{a}\frac{\partial a_1}{\partial z} = \frac{\varepsilon}{a\ell h}\left[\frac{\partial^2}{\partial\tau\partial z}\left(\frac{\xi}{h}\right) + \bar{B}\frac{\partial\eta}{\partial z}\right] + O\left(\frac{1}{a}\frac{\varepsilon^2}{\ell^2}\right). \tag{A.14}$$

From the expression (A.3) for the in-plane strain tensor $\gamma_{\alpha\beta}$ we obtain:

$$\gamma_{11} = \frac{\varepsilon}{\ell h}\left(-\xi\bar{B} + \frac{\partial}{\partial\tau}\left(\frac{\eta}{h}\right)\right) + O\left(\frac{\varepsilon^2}{\ell^2}\right), \tag{A.15}$$

$$\gamma_{12} = \gamma_{21} = \frac{1}{2}\frac{\varepsilon}{\ell h}\left(\frac{\partial\eta}{\partial z} + \frac{\partial\zeta}{\partial\tau}\right) + O\left(\frac{\varepsilon^2}{\ell^2}\right), \tag{A.16}$$

$$\gamma_{22} = \frac{\varepsilon}{\ell}\frac{\partial\zeta}{\partial z} + O\left(\frac{\varepsilon^2}{\ell^2}\right). \tag{A.17}$$

Finally, from the expression (A.3) for $\kappa_{\alpha\beta}$, we obtain:

$$\kappa_{11} = \frac{\varepsilon}{a\ell h}\left[\bar{B}\left(-\xi\bar{B}+\frac{\partial}{\partial\tau}\left(\frac{\eta}{h}\right)\right)-\frac{\partial}{\partial\tau}\left(\frac{\eta\bar{B}}{h}+\frac{1}{h}\frac{\partial}{\partial\tau}\left(\frac{\xi}{h}\right)\right)\right]+O\left(\frac{1}{a}\frac{\varepsilon^2}{\ell^2}\right), \quad \text{(A.18)}$$

$$\kappa_{12} = -\frac{\varepsilon}{a\ell h}\left[\frac{\partial}{\partial\tau}\left(\frac{1}{h}\frac{\partial\xi}{\partial z}\right)-\bar{B}\frac{\partial\zeta}{\partial\tau}\right]+O\left(\frac{1}{a}\frac{\varepsilon^2}{\ell^2}\right), \quad \text{(A.19)}$$

$$\kappa_{21} = -\frac{\varepsilon}{a\ell h}\left[\frac{\partial}{\partial\tau}\left(\frac{1}{h}\frac{\partial\xi}{\partial z}\right)+\bar{B}\frac{\partial\eta}{\partial z}\right]+O\left(\frac{1}{a}\frac{\varepsilon^2}{\ell^2}\right), \quad \text{(A.20)}$$

$$\kappa_{22} = -\frac{\varepsilon}{a\ell h}\frac{\partial^2\xi}{\partial z^2}+O\left(\frac{1}{a}\frac{\varepsilon^2}{\ell^2}\right). \quad \text{(A.21)}$$

A.6. *Components of the in-plane stress $N^{\alpha\beta}$*

The in-plane stress is given by (A.4). The components must be evaluated in terms of the displacement functions (ξ,η,ζ). The calculations have already been completed by Whittaker (2015), so we just quote their results in (3.5).

A.7. *Components of the bending stress $M^{\alpha\beta}$*

The bending stress is given by (A.5). We wish to express the components of $M^{\alpha\beta}$ in terms of ξ, η, ζ, to $O(\varepsilon)$ accuracy. We note that $a_{\alpha\beta}$ and $b_{\alpha\beta}$ always appear in (A.5) multiplied by an $O(\varepsilon)$ quantity, so we

need only retain the $O(1)$ parts of these two tensors: $\bar{a}_{11} = \bar{a}_{22} = 1$ and $\bar{b}_{11} = \bar{b}_1^1 = \bar{B}/a$. We then have

$$
\begin{aligned}
M^{11} &= K\Big[-(1-\nu)(\bar{b}_1^1\gamma^{11} - \bar{b}_1^1\gamma^{11}) - \nu(\bar{b}^{11} - \bar{b}_1^1)(\gamma_1^1 + \gamma_2^2) \\
&\qquad + (1-\nu)\kappa^{11} + \nu(\kappa_1^1 + \kappa_2^2)\Big] + O\left(\frac{K}{a}\frac{\varepsilon^2}{\ell^2}\right), \tag{A.22}\\
&= K\big(\kappa^{11} + \nu\kappa^{22}\big) + O\left(\frac{K}{a}\frac{\varepsilon^2}{\ell^2}\right), \tag{A.23}\\
&= \frac{\varepsilon K}{a\ell h}\Big[\bar{B}\Big(-\xi\bar{B} + \frac{\partial}{\partial\tau}\Big(\frac{\eta}{h}\Big)\Big) \\
&\qquad - \frac{\partial}{\partial\tau}\Big(\frac{\eta\bar{B}}{h} + \frac{1}{h}\frac{\partial}{\partial\tau}\Big(\frac{\xi}{h}\Big)\Big) - \nu\frac{\partial^2\xi}{\partial z^2}\Big] + O\left(\frac{K}{a}\frac{\varepsilon^2}{\ell^2}\right), \tag{A.24}\\
M^{12} &= K\Big[-(1-\nu)(\bar{b}_1^1\gamma^{12} - \bar{b}_1^1\gamma^{12}) - \nu(b^{12} - b_1^1)(\gamma_1^1 + \gamma_2^2) \\
&\qquad + \tfrac{1}{2}(1-\nu)(\kappa^{12} + \kappa^{21})\Big] + O\left(\frac{K}{a}\frac{\varepsilon^2}{\ell^2}\right), \tag{A.25}\\
&= \tfrac{1}{2}K(1-\nu)(\kappa^{12} + \kappa^{21}) + O\left(\frac{K}{a}\frac{\varepsilon^2}{\ell^2}\right), \tag{A.26}\\
&= \frac{\varepsilon K}{a\ell h}(1-\nu)\Big[-\frac{\partial^2}{\partial\tau\partial z}\Big(\frac{\xi}{h}\Big) + \frac{\bar{B}}{2}\Big(\frac{\partial\zeta}{\partial\tau} - \frac{\partial\eta}{\partial z}\Big)\Big] + O\left(\frac{K}{a}\frac{\varepsilon^2}{\ell^2}\right), \tag{A.27}\\
M^{21} &= K\Big[-(1-\nu)(-\bar{b}_1^1\gamma^{21}) + \tfrac{1}{2}(1-\nu)(\kappa^{21} + \kappa^{12})\Big] + O\left(\frac{K}{a}\frac{\varepsilon^2}{\ell^2}\right), \tag{A.28}\\
&= K(1-\nu)\Big[\frac{\bar{B}}{a}\gamma^{21} + \tfrac{1}{2}(\kappa^{12} + \kappa^{21})\Big] + O\left(\frac{K}{a}\frac{\varepsilon^2}{\ell^2}\right), \tag{A.29}\\
&= \frac{\varepsilon K}{a\ell h}(1-\nu)\Big[-\frac{\partial^2}{\partial\tau\partial z}\Big(\frac{\xi}{h}\Big) + \bar{B}\frac{\partial\zeta}{\partial\tau}\Big] + O\left(\frac{K}{a}\frac{\varepsilon^2}{\ell^2}\right), \tag{A.30}\\
M^{22} &= K\Big[-(1-\nu)(-\bar{b}_1^1\gamma^{22}) - \nu(-\bar{b}_1^1)(\gamma_1^1 + \gamma_2^2) \\
&\qquad + (1-\nu)\kappa^{22} + \nu(\kappa_1^1 + \kappa_2^2)\Big] + O\left(\frac{K}{a}\frac{\varepsilon^2}{\ell^2}\right), \tag{A.31}\\
&= K\Big[\frac{\bar{B}}{a}(\gamma_{22} + \nu\gamma_{11}) + (\kappa_{22} + \nu\kappa_{11})\Big] + O\left(\frac{K}{a}\frac{\varepsilon^2}{\ell^2}\right), \tag{A.32}\\
&= \frac{\varepsilon K}{a\ell h}\Big[h\bar{B}\frac{\partial\zeta}{\partial z} + 2\nu\bar{B}\Big(-\xi\bar{B} + \frac{\partial}{\partial\tau}\Big(\frac{\eta}{h}\Big)\Big) \\
&\qquad - \frac{\partial^2\xi}{\partial z^2} - \nu\frac{\partial}{\partial\tau}\Big(\frac{\eta\bar{B}}{h} + \frac{1}{h}\frac{\partial}{\partial\tau}\Big(\frac{\xi}{h}\Big)\Big)\Big] + O\left(\frac{K}{a}\frac{\varepsilon^2}{\ell^2}\right). \tag{A.33}
\end{aligned}
$$

A.8. *Displacement recovery from the components of the stress tensor*

Whittaker (2015) derived the following expressions to recover the leading-order displacement variables from the three leading-order components ($\tilde{N}$, $\tilde{S}$ and $\tilde{\Sigma}$) of the in-plane stress tensor:

$$
\begin{align}
\zeta(\tau,z) &= \frac{1}{12(1-\nu^2)} \int_0^z \left(\tilde{\Sigma}(\tau,z') - \nu\tilde{N}(\tau,z') \right) dz', \tag{A.34} \\
\eta(\tau,z) &= \int_0^z \left(\frac{2h(\tau)\tilde{S}(\tau,z')}{12(1-\nu)} - \frac{\partial \zeta(\tau,z')}{\partial \tau} \right) dz', \tag{A.35} \\
\xi(\tau,z) &= -\frac{h(\tau)}{\bar{B}(\tau)} \left(\frac{\tilde{N}(\tau,z) - \nu\tilde{\Sigma}(\tau,z)}{12(1-\nu^2)} - \frac{1}{h(\tau)} \frac{\partial}{\partial \tau} \left(\frac{\eta(\tau,z)}{h(\tau)} \right) \right). \tag{A.36}
\end{align}
$$

These results are utilised in the present work.

B. The outer shear layer in Regime Ia

For a boundary-layer of width $\delta \gg 1$ in this regime, we defer to the analysis in Whittaker (2015), where the bulk solution with $\delta = O(\ell)$ and an outer shear layer with $\delta = O(\tilde{\mathscr{F}}^{-1/2})$ are found. This is appropriate for Regime Ia since $1 \ll \tilde{\mathscr{F}}^{-1/2} \ll \ell$.

Whittaker (2015) only considered transmural pressures that are even and π-periodic in τ, leading to deformations have mirror symmetry in the x and y axes. It is possible to relax this and consider more general deformations, but we retain this restriction here for simplicity.

With this symmetry restriction, Whittaker (2015) showed that the solution in the outer shear layer can be written as a sum over azimuthal eigenmodes $Y_n(\tau)$ which are odd and π-periodic in τ. These eigenmodes satisfy the eigenvalue equation

$$
\mathscr{L}(Y_n) = \mu_n^2 Y_n \qquad \text{for } n = 1, 2, 3, \ldots \tag{B.1}
$$

where the linear operator $\mathscr{L}$ is given by

$$
\mathscr{L} \equiv \frac{1}{h} \frac{\partial}{\partial \tau} \frac{1}{h} \frac{\partial}{\partial \tau} \left(\frac{1}{\bar{B}^2 h} \frac{\partial}{\partial \tau} \frac{1}{h} \frac{\partial}{\partial \tau} - 1 \right) \tag{B.2}
$$

and $0 = \mu_0 < \mu_1 < \mu_2 < \cdots$. The operator $\mathscr{L}$ is self-adjoint with respect to the inner product $\langle u, v \rangle = \int_0^{2\pi} uvh \, d\tau$ and so its eigenfunctions form a complete set. We chose to normalise the eigenfunctions so that $\langle Y_n, Y_n \rangle = 1$. This means we have

$$
\langle Y_n, Y_m \rangle \equiv \int_0^{2\pi} Y_n(\tau) Y_m(\tau) h(\tau) \, d\tau = \delta_{nm}, \tag{B.3}
$$

where δ_{nm} is the Kronecker delta.

Taking the general solutions from Whittaker (2015) and applying only the conditions that arise from matching with the bulk exterior solution, the leading-order stresses in the outer shear layer are given by

$$
\begin{align}
\tilde{N} &= \tilde{\mathscr{F}}^{3/2} \sum_{n=1}^{\infty} \frac{\breve{B}_n}{\bar{B}^2 h} \frac{\partial}{\partial \tau} \left(\frac{1}{h} \frac{\partial Y_n}{\partial \tau} \right) e^{-\mu_n \breve{z}} + \ldots, \tag{B.4} \\
\tilde{S} &= \tilde{\mathscr{F}} \sum_{n=1}^{\infty} \frac{\breve{B}_n}{\mu_n h} \frac{\partial}{\partial \tau} \left(\frac{1}{\bar{B}^2 h} \frac{\partial}{\partial \tau} \frac{1}{h} \frac{\partial Y_n}{\partial \tau} - Y_n \right) e^{-\mu_n \breve{z}} + \ldots, \tag{B.5} \\
\tilde{\Sigma} &= \tilde{\mathscr{F}}^{1/2} \sum_{n=1}^{\infty} \breve{B}_n Y_n(\tau) e^{-\mu_n \breve{z}} + \ldots, \tag{B.6}
\end{align}
$$

where $\check{z} = z/\tilde{\mathscr{F}}^{-1/2}$, the $\check{B}_n$ are a set of constants giving the amplitude of each mode. The displacements in the outer shear layer are recovered from these expressions using (A.34)–(A.36). Again, we apply only the conditions that arise from matching with the bulk exterior solution, and obtain, to leading order,

$$\xi = \frac{\tilde{\mathscr{F}}^{-1/2}}{12(1-\nu^2)\bar{B}(\tau)} \sum_{n=1}^{\infty} \left\{ \frac{\check{B}_n}{\mu_n} \left[\frac{1}{\mu_n}\left(1 - e^{-\mu_n \check{z}}\right) - \check{z} \right] + \check{E}_n + \check{D}_n\check{z} \right\} \left(\frac{Y_n'}{h} \right)', \qquad (B.7)$$

$$\eta = \frac{\tilde{\mathscr{F}}^{-1/2}}{12(1-\nu^2)} \sum_{n=1}^{\infty} \left\{ \frac{\check{B}_n}{\mu_n} \left[\frac{1}{\mu_n}\left(1 - e^{-\mu_n \check{z}}\right) - \check{z} \right] + \check{E}_n + \check{D}_n\check{z} \right\} Y_n'(\tau), \qquad (B.8)$$

$$\zeta = \frac{1}{12(1-\nu^2)} \left\{ \check{D}_0 + \sum_{n=1}^{\infty} \left[\frac{\check{B}_n}{\mu_n}\left(1 - e^{-\mu_n \check{z}}\right) + \check{D}_n \right] Y_n(\tau) \right\}, \qquad (B.9)$$

where the $\check{D}_n$ and $\check{E}_n$ are additional set of constants giving the amplitudes of further modes. (There is no $\check{E}_0$ constant term in the expression for η since the assumed symmetry requires η to be an odd function of τ.)

The constants $\check{B}_n$, $\check{D}_n$ and $\check{E}_n$ appear in matching conditions with the bulk solution in the rest of the tube and the intermediate solution of §5.

C. Bulk shear-layer solution in Regimes Ib and Iab

In Regimes Ib and Iab, the estimated $O(\tilde{\mathscr{F}}^{-1/2})$ thickness of the outer shear layer from Whittaker (2015) is greater than or comparable with the length ℓ of the elastic tube. Hence the bulk interior solution comprises a modified form of the outer shear layer, in which the transmural pressure is also present at leading order. In this appendix, we solve for the displacements in this bulk region.

In Whittaker (2015), the outer shear layer was forced by the matching with the bulk interior solution. The amplitude of the deformations was such that the transmural pressure did not contribute in the outer shear layer at leading order. Now there is no separate bulk interior solution to force the displacements in the outer shear layer. The displacement amplitude in the bulk shear layer is reduced, so that the leading-order terms in the normal equilibrium equation have the same magnitude as the transmural pressure.

We now follow the outer shear layer derivation in Whittaker (2015), but using slightly adjusted scalings to account for the $O(\ell)$ axial length scale and the altered amplitude of the displacements. We define scaled variables for the axial coordinate, hoop stress, axial stress and in-plane shear stress as:

$$\hat{z} = \frac{z}{\ell}, \qquad \hat{N} = \frac{\tilde{N}}{\mathscr{P}}, \qquad \hat{\Sigma} = \frac{\tilde{\Sigma}}{\ell^2 \mathscr{P}}, \qquad \hat{S} = \frac{\tilde{S}}{\ell \mathscr{P}}. \qquad (C.1)$$

where $\mathscr{P}$ is the dimensionless pressure scale defined in (3.24). These scales arise from altering the axial length scale from $\mathscr{F}^{-1/2}$ to ℓ in the Ia outer-shear-layer scales in (B.4)–(B.6), and then scaling the three stresses by a factor of $\ell^3 \mathscr{P}$ in order for the forcing from the transmural pressure to appear at leading order.

Substituting the scales (C.1) into (A.34)–(A.36) we obtain leading-order expressions for the displacements in terms of the scaled stresses:

$$\zeta_{\hat{z}} \sim \frac{\ell^3 \mathscr{P}}{12(1-\nu^2)}\hat{\Sigma}, \qquad \eta_{\hat{z}\hat{z}} \sim -\frac{\ell^4 \mathscr{P}h}{12(1-\nu^2)}\hat{\Sigma}_\tau, \qquad \xi_{\hat{z}\hat{z}} \sim -\frac{\ell^4 \mathscr{P}h}{12\bar{B}(1-\nu^2)}\hat{\Sigma}_{\tau\tau}, \qquad (C.2)$$

where subscripts denote partial derivatives, but a subscript τ represents the operator $h^{-1}\partial/\partial\tau$.

Then, substituting (C.1) and (C.2) into (3.21)–(3.23), we obtain the following leading-order equations governing the bulk shear layer:

$$-\hat{N} + (\ell^2 \tilde{\mathscr{F}})\bar{B}^{-2}\hat{\Sigma}_{\tau\tau} = \bar{B}^{-1}\tilde{p}, \tag{C.3}$$

$$\hat{N}_\tau + \hat{S}_{\hat{z}} - (\ell^2 \tilde{\mathscr{F}})\hat{\Sigma}_\tau = 0, \tag{C.4}$$

$$\hat{S}_\tau + \hat{\Sigma}_{\hat{z}} = 0, \tag{C.5}$$

Equations (C.3)–(C.5) differ from those in Whittaker (2015) for the outer shear layer only by the presence of the $\tilde{p}$ forcing term on the right-hand side of the first equation, and the factors of $\ell^2 \tilde{\mathscr{F}}$ multiplying the two $\hat{\Sigma}_{\tau\tau}$ terms.

In Regime Ib, we have $\ell^2 \tilde{\mathscr{F}} \ll 1$, so the terms containing $\ell^2 \tilde{\mathscr{F}}$ are asymptotically small and can be neglected. However, we shall retain these terms in the working here, to simultaneously cover the case of Regime Iab, where $\ell^2 \tilde{\mathscr{F}} = O(1)$.

For simplicity, we restrict attention here to the case where $\tilde{p}$ is even and π-periodic in τ. The stresses $\hat{N}$ and $\hat{\Sigma}$ and the displacements ξ and ζ then share this symmetry, while $\hat{S}$ and η are odd and π-periodic in τ.

Eliminating $\hat{S}$ between (C.4) and (C.5), we obtain

$$-\hat{N}_{\tau\tau} + (\ell^2 \tilde{\mathscr{F}})\hat{\Sigma}_{\tau\tau} + \hat{\Sigma}_{\hat{z}\hat{z}} = 0. \tag{C.6}$$

Then, eliminating $\hat{N}$ between (C.3) and (C.6) yields

$$\hat{\Sigma}_{\hat{z}\hat{z}} - (\ell^2 \tilde{\mathscr{F}})\mathscr{L}(\hat{\Sigma}) = -\left(\bar{B}^{-1}\tilde{p}\right)_{\tau\tau}, \tag{C.7}$$

where $\mathscr{L}$ is the operator from Whittaker (2015) defined here in (B.2). As before, we represent the eigenfunctions of $\mathscr{L}$ by $Y_n(\tau)$ for $n = 0, 1, 2, \ldots$, with corresponding eigenvalues μ_n^2, where $0 = \mu_0 < \mu_1 < \mu_2 < \cdots$. We have the same orthogonality and normalisation as in (B.3).

From the completeness, orthogonality and normalisation of the eigenfunctions, if we define

$$Q_n = \left\langle \left(\bar{B}^{-1}\tilde{p}\right)_{\tau\tau}, Y_n \right\rangle \equiv \int_0^{2\pi} \left(\bar{B}^{-1}\tilde{p}\right)_{\tau\tau} Y_n h\, d\tau, \tag{C.8}$$

then we have that

$$\left(\bar{B}^{-1}\tilde{p}\right)_{\tau\tau} = \sum_{n=1}^{\infty} Q_n(\hat{z})Y_n(\tau). \tag{C.9}$$

(The $n = 0$ term is not needed in (C.9) since $Q_0 = 0$. This can be seen by noting that $Y_0(\tau)$ is constant in τ, and then using integration by parts in (C.8) when $n = 0$.)

We now introduce $q_n(\hat{z})$ as the general solutions of the ordinary differential equations

$$q_0''' = 0, \qquad q_n'''' - (\ell^2 \tilde{\mathscr{F}}\mu_n^2)q_n'' = -Q_n(\hat{z}) \quad (n = 1, 2, 3, \ldots). \tag{C.10}$$

The general solution of (C.7) for $\hat{\Sigma}$ can then be written in terms of the eigenfunctions and the q_n as

$$\hat{\Sigma} = q_0'(\hat{z}) + \sum_{n=1}^{\infty} Y_n(\tau)q_n''(\hat{z}). \tag{C.11}$$

Noting that $\mu_n^2 Y_n = \mathscr{L}(Y_n) = (\bar{B}^{-2} Y_{n\tau\tau} - Y_n)_{\tau\tau}$, we can integrate (C.9) twice with respect to τ to obtain

$$\bar{B}^{-1}\tilde{p} = Q_0^*(\hat{z}) + \sum_{n=1}^{\infty} \frac{Q_n}{\mu_n^2}\left(\frac{1}{\bar{B}^2 h}\frac{\partial}{\partial \tau}\frac{1}{h}\frac{\partial Y_n}{\partial \tau} - Y_n\right). \tag{C.12}$$

The new function $Q_0^*(\hat{z})$ is one of the 'constants' of integration. It must be set in terms of $\tilde{p}$ and the Q_n to ensure that equality holds in (C.12). The other constant of integration is necessarily zero, due to the periodicity of all the other terms.

Using the expressions for $\hat{\Sigma}$ in (C.11) and $\bar{B}^{-1}\tilde{p}$ in (C.12), we can recover $\hat{N}$ using (C.3). After eliminating $Q_n(\hat{z})$ in favour of $q_n(\hat{z})$ using (C.10), we obtain

$$\hat{N} = -Q_0^*(\hat{z}) + \sum_{n=1}^{\infty}\left\{\frac{1}{\bar{B}^2 h}\frac{\partial}{\partial \tau}\left(\frac{1}{h}\frac{\partial Y_n}{\partial \tau}\right)\frac{q_n''''(\hat{z})}{\mu_n^2} + Y_n(\tau)\left((\ell^2\tilde{\mathscr{F}})q_n''(\hat{z}) - \frac{q_n''''(\hat{z})}{\mu_n^2}\right)\right\}. \tag{C.13}$$

Similarly, $\hat{S}$ is recovered using (C.4) and (C.5), giving

$$\hat{S} = S_0^* - \left(\int_0^{\tau} h(\tau')\,d\tau'\right)q_0''(\hat{z}) - \sum_{n=1}^{\infty}\frac{1}{\mu_n^2 h}\frac{\partial}{\partial \tau}\left(\frac{1}{\bar{B}^2 h}\frac{\partial}{\partial \tau}\frac{1}{h}\frac{\partial Y_n}{\partial \tau} - Y_n\right)q_n'''(\hat{z}), \tag{C.14}$$

where S_0^* is an arbitrary constant of integration. To ensure $\hat{S}$ is odd and periodic in τ, we must have

$$S_0^* = 0, \qquad q_0''(\hat{z}) \equiv 0. \tag{C.15}$$

Hence

$$\hat{S} = -\sum_{n=1}^{\infty}\frac{1}{\mu_n^2 h}\frac{\partial}{\partial \tau}\left(\frac{1}{\bar{B}^2 h}\frac{\partial}{\partial \tau}\frac{1}{h}\frac{\partial Y_n}{\partial \tau} - Y_n\right)q_n'''(\hat{z}). \tag{C.16}$$

The leading-order displacements can then be recovered by substituting (C.11) into (C.2). We obtain

$$\zeta \sim \frac{\ell^3\mathscr{P}}{12(1-\nu^2)}\left\{q_0(\hat{z}) + \sum_{n=1}^{\infty}Y_n(\tau)\,q_n'(\hat{z})\right\}, \tag{C.17}$$

$$\eta \sim -\frac{\ell^4\mathscr{P}}{12(1-\nu^2)}\sum_{n=1}^{\infty}\frac{\partial Y_n}{\partial \tau}q_n(\hat{z}), \tag{C.18}$$

$$\xi \sim -\frac{\ell^4\mathscr{P}}{12(1-\nu^2)\bar{B}}\sum_{n=1}^{\infty}\frac{\partial}{\partial \tau}\frac{1}{h}\frac{\partial Y_n}{\partial \tau}q_n(\hat{z}). \tag{C.19}$$

The constants of integration that would have been expected to appear in the first two expressions are already accounted for by the generality of the solution for q_n, given the symmetries of ζ and η.

At this point, the solution is still undetermined, since we do not have any boundary conditions on $q_n(\hat{z})$ for the ODEs (C.10). These missing boundary conditions will be determined when the solutions are matched with the boundary-layer solutions as $\hat{z} \to 0$ and $\hat{z} \to 1$.

We can, however, use (C.19) to set ε, the scale for the normal displacements in the bulk. Referring to (2.9), we require that $\xi = O(\ell)$ when $\hat{z} = O(1)$, which means we must have $\mathscr{P} = O(\ell^{-3})$. Referring to (3.24), we can achieve this by setting

$$\varepsilon = \frac{\vartheta^2\ell^4 a^3 P}{K} \qquad \Rightarrow \qquad \mathscr{P} = \ell^{-3}. \tag{C.20}$$

D. Exact solution in the limit of a circular cross-section

We consider the special case of a base state with a circular cross section. This corresponds to the limit $\sigma_0 \to \infty$. Then $h(\tau) \equiv 1$, $\bar{B}(\tau) \equiv -1$. The equations (3.21)–(3.23) then become

$$\vartheta^2\left(\tilde{M}^{11}_{\tau\tau} + \tilde{M}^{12}_{\tau z} + \tilde{M}^{21}_{z\tau} + \tilde{M}^{22}_{zz}\right) - \tilde{N} + 12(1-\nu^2)\tilde{\mathscr{F}}\xi_{zz} = -\mathscr{P}\,\tilde{p}, \tag{D.1}$$

$$\left(\tilde{N}_\tau + \tilde{S}_z\right) + 12(1-\nu^2)\tilde{\mathscr{F}}\eta_{zz} + \vartheta^2\left(\tilde{M}^{11}_\tau + \tilde{M}^{21}_z\right) = 0, \tag{D.2}$$

$$\left(\tilde{S}_\tau + \tilde{\Sigma}_z\right) + 12(1-\nu^2)\tilde{\mathscr{F}}\left(\xi_z + \eta_{\tau z} + 2\zeta_{zz}\right) = 0, \tag{D.3}$$

where $(\,\cdot\,)_z \equiv \partial/\partial z$ as before, but we now have $(\,\cdot\,)_\tau \equiv \partial/\partial\tau$.

Due to the periodicity and symmetry, and the constant coefficients in the equations, the τ dependence can be captured in Fourier modes, which then decouple. For a transmural pressure

$$\tilde{p} = \sum_{n=0}^{\infty} p_n(z)\cos(2n\tau), \tag{D.4}$$

we write

$$\xi = \sum_{n=0}^{\infty} \xi_n(z)\cos(2n\tau), \qquad \eta = \sum_{n=0}^{\infty} \eta_n(z)\sin(2n\tau), \qquad \zeta = \sum_{n=0}^{\infty} \zeta_n(z)\cos(2n\tau). \tag{D.5}$$

Then, from (3.10)–(3.12), the stresses are given by

$$\tilde{N} = 12\sum_{n=0}^{\infty}\left(\xi_n + 2n\eta_n + \nu\zeta'_n\right)\cos(2n\tau), \tag{D.6}$$

$$\tilde{S} = 6(1-\nu)\sum_{n=0}^{\infty}\left(\eta'_n - 2n\zeta_n\right)\sin(2n\tau), \tag{D.7}$$

$$\tilde{\Sigma} = 12\sum_{n=0}^{\infty}\left(\zeta'_n + \nu(\xi_n + 2n\eta_n)\right)\cos(2n\tau); \tag{D.8}$$

and from (3.13)–(3.16) the bending moments are

$$\tilde{M}^{11} = \sum_{n=0}^{\infty}\left(-\xi_n + 4n^2\xi_n - \nu\xi''_n\right)\cos(2n\tau), \tag{D.9}$$

$$\tilde{M}^{12} = \frac{1-\nu}{2}\sum_{n=0}^{\infty}\left(4n\xi'_n + \eta'_n + 2n\zeta_n\right)\sin(2n\tau), \tag{D.10}$$

$$\tilde{M}^{21} = (1-\nu)\sum_{n=0}^{\infty}2n\left(\xi'_n + \zeta_n\right)\sin(2n\tau), \tag{D.11}$$

$$\tilde{M}^{22} = \sum_{n=0}^{\infty}\left((4n^2-1-2\nu)\xi_n - \xi''_n - 2n\nu\eta_n\right)\cos(2n\tau). \tag{D.12}$$

Substituting these forms into the equilibrium equations (3.21)–(3.23), the system decouples, and for each $n \in \{0, 1, 2, \ldots\}$ we have

$$-\vartheta^2 \frac{\partial^4 \xi_n}{\partial z^4} + \left[(4(3-\nu)n^2 - 2\nu - 1)\vartheta^2 + 12\tilde{\mathscr{F}}(1-\nu^2)\right]\frac{\partial^2 \xi_n}{\partial z^2}$$
$$- \vartheta^2(3\nu - 1)n\frac{\partial^2 \eta_n}{\partial z^2} + \left[6n^2(1-\nu)\vartheta^2 - 12\nu\right]\frac{\partial \zeta_n}{\partial z}$$
$$- \left[12 + 4n^2(4n^4 - 1)\vartheta^2\right]\xi_n - 24n\,\eta_n = -\mathscr{P}p_n, \quad \text{(D.13)}$$

$$2n\vartheta^2 \frac{\partial^2 \xi_n}{\partial z^2} + \left[12\tilde{\mathscr{F}}(1-\nu^2) + 6(1-\nu)\right]\frac{\partial^2 \eta_n}{\partial z^2}$$
$$+ 2n\left((1-\nu)\vartheta^2 - 6(1+\nu)\right)\frac{\partial \zeta_n}{\partial z}$$
$$- 2n\left((4n^2 - 1)\vartheta^2 + 12\right)\xi_n + 48n^2\eta_n = 0, \quad \text{(D.14)}$$

$$\left[2\tilde{\mathscr{F}}(1-\nu^2) + 1\right]\frac{\partial^2 \zeta_n}{\partial z^2} + \left[\tilde{\mathscr{F}}(1-\nu^2) + \nu\right]\frac{\partial \xi_n}{\partial z}$$
$$+ n\left[2\tilde{\mathscr{F}}(1-\nu^2) + (1+\nu)\right]\frac{\partial \eta_n}{\partial z} - 2n^2(1-\nu)\zeta_n = 0, \quad \text{(D.15)}$$

apart from $n = 0$, where the azimuthal equation (D.14) is absent. From (2.11), the boundary conditions are

$$\xi_n(z) = \eta_n(z) = \zeta_n(z) = \xi'_n(z) = 0 \quad \text{at} \quad z = 0, \ell, \quad \text{(D.16)}$$

except for $n = 0$, where the condition on η_0 is absent.

For each n, this is a coupled set of forced linear ordinary differential equations with constant coefficients. It is amenable to solution by the standard solution technique of seeking a particular integral and a complimentary function made up of a sum of terms of the form e^{kz}.

For simplicity we now concentrate on the case where each $p_n(z)$ is uniform in z. For $n > 0$, the system is 8th order, and the solution takes the form

$$\xi_n(z) = A_n^{(0)} + \sum_{i=1}^{4} A_n^{(i)}\left(e^{-k_n^{(i)}(\ell-z)} + e^{-k_n^{(i)}z}\right), \quad \text{(D.17)}$$

$$\eta_n(z) = B_n^{(0)} + \sum_{i=1}^{4} B_n^{(i)}\left(e^{-k_n^{(i)}(\ell-z)} + e^{-k_n^{(i)}z}\right), \quad \text{(D.18)}$$

$$\zeta_n(z) = \sum_{i=1}^{4} C_n^{(i)}\left(e^{-k_n^{(i)}(\ell-z)} - e^{-k_n^{(i)}z}\right), \quad \text{(D.19)}$$

where $A_n^{(i)}$, $B_n^{(i)}$, $C_n^{(i)}$, and $k_n^{(i)} > 0$ are constants, and the $\left(k_n^{(i)}\right)^2$ are the roots of a 4th-order polynomial. (The $z \leftrightarrow \ell - z$ symmetry in the system means the values of k occur in positive/negative pairs, and the solution is symmetric about $z = \ell/2$.)

The constants $A_n^{(0)}$ and $B_n^{(0)}$ are the particular integral for (D.13)–(D.15), and are found to be given by

$$A_n^{(0)} = \frac{\mathscr{P}\, p_n}{\left(4n^2-1\right)^2 \vartheta^2}, \qquad B_n^{(0)} = -\frac{\left(\left(4n^2-1\right)\vartheta^2+12\right)\mathscr{P}\, p_n}{24n\left(4n^2-1\right)^2\vartheta^2}. \tag{D.20}$$

The sums in (D.17)–(D.19) represent the complementary function for the ODE system. For each $i \in \{1,2,3,4\}$, the equations (D.13)–(D.15) determine $B_n^{(i)}$ and $C_n^{(i)}$ in terms of $A_n^{(i)}$. The four boundary conditions (D.16) then determine the $A_n^{(i)}$.

For $n=0$, we instead have a 6th-order system. The solution procedure is similar, except η_0 does not contribute, (D.14) is absent, and there are only three pairs of roots $\pm k_n^{(i)}$. The particular integral is given by

$$A_0^{(0)} = \frac{\mathscr{P}\, p_0}{12}, \tag{D.21}$$

while $B_0^{(0)}$ is not required. For each $i \in \{1,2,3\}$, the equations (D.13) and (D.15) determine $C_0^{(i)}$ in terms of $A_0^{(i)}$. The three boundary conditions in (D.16) that do not involve η_0 then determine the $A_0^{(i)}$.

These solutions can, in principle, be computed purely analytically in terms of the parameters v, ℓ, $\tilde{\mathscr{F}}$, ϑ, and $\mathscr{P}$. However, the resulting expressions are extremely unwieldy. So instead, we use Maple to compute the general polynomial for k_n symbolically, before substituting in specific parameter values. Maple is then used to compute numerical values for the roots $k_n^{(i)}$, and then the coefficients $A_n^{(i)}$, $B_n^{(i)}$, $C_n^{(i)}$. The full solutions can then be constructed from (D.5) and (D.17)–(D.19). Results are compared with the asymptotic solutions in §10.

E. Regime Ia asymptotic bulk solution in the circular limit

Netherwood & Whittaker (2023) considered an extension to the idea of a 'tube law' to govern the perturbation in the bulk of a finite-length elastic-walled tube, with an initially elliptical cross-section subjected to a transmural pressure that is even and π-periodic in τ. They used an expansion for η in terms of a set of azimuthal eigenfunctions $W_n(\tau)$ and axially varying amplitudes $a_n(z)$:

$$\eta(\tau,z) = \ell \sum_{n=1}^{\infty} a_n(z) W_n(\tau), \tag{E.1}$$

where the $W_n(\tau)$ are the normalised solutions of a generalised eigenvalue problem, and each amplitude satisfies $a_n(0) = a_n(\ell) = 0$.[3]

Using this expansion, Netherwood & Whittaker (2023) obtained tube-law like expressions governing each $a_n(z)$:

$$\mathscr{F}\ell^2 \frac{\mathrm{d}^2 a_n}{\mathrm{d}z^2} - \lambda_n a_n = Q_n, \tag{E.2}$$

where λ_n is the eigenvalue corresponding to $W_n(\tau)$, and

$$Q_n = \tanh^2(2\sigma_0)\int_0^{\pi/2} \frac{1}{h}\frac{\partial}{\partial\tau}\left(\frac{\tilde{p}}{\bar{B}}\right)W_n\,\mathrm{d}\tau. \tag{E.3}$$

---

[3] Netherwood & Whittaker (2023) used a different scaling for the displacements, which explains the additional factor of ℓ in (E.1). They also used the notation $Y_n(\tau)$ for these eigenfunctions, but in the present work, $Y_n(\tau)$ corresponds to a different set of eigenfunctions.

In the circular limit $\sigma_0 = \infty$, we have $\bar{B} = -1$ and $h = 1$. In this limit, Netherwood & Whittaker (2023) showed that the limiting forms of the eigenfunctions and eigenvalues are

$$W_n(\tau) = \frac{2\sin(2n\tau)}{\sqrt{\pi(4n^2+1)}}, \qquad \lambda_n = \frac{4n^2(4n^2-1)^2}{4n^2+1}. \tag{E.4}$$

So in the circular limit, with a pressure forcing of $\tilde{p} = -\cos(2m\tau)$ for $m \in \mathbb{Z}^+$, the orthogonality of the trigonometric functions in (E.3) means that only the mth mode is excited, i.e. $Q_n = 0$ for $n \neq m$. From (E.1)–(E.4), the solution for η is then

$$\eta(\tau, z) = \ell a(z) \frac{2\sin(2m\tau)}{\sqrt{\pi(4m^2+1)}}, \tag{E.5}$$

where $a(z)$ is the solution of the linear two-point boundary-value problem

$$\mathscr{F}\ell^2 \frac{\mathrm{d}^2 a}{\mathrm{d}z^2} - \lambda_m a = -\frac{m\sqrt{\pi}}{\sqrt{4m^2+1}}, \qquad a(0) = a(\ell) = 0. \tag{E.6}$$

Solving (E.6) for $a(z)$ and inserting into (E.5), we obtain

$$\eta(\tau, z) = \frac{\ell}{2m(4m^2-1)^2}\left[1 - \frac{\cosh\left(k(z-\frac{1}{2}\ell)\right)}{\cosh\left(\frac{1}{2}k\ell\right)}\right]\sin(2m\tau), \tag{E.7}$$

where

$$k = \sqrt{\frac{\lambda_m}{\mathscr{F}\ell^2}} = \frac{2m(4m^2-1)}{\sqrt{4m^2+1}}\frac{\vartheta\tilde{\mathscr{F}}^{-1/2}}{\sqrt{12(1-\nu^2)}}. \tag{E.8}$$

Netherwood & Whittaker (2023) provided equations for the recovery of the other two displacement variables from $\eta(\tau, z)$:

$$\xi\sinh(2\sigma_0) + \frac{2h^2}{c^2}\frac{\partial\eta}{\partial\tau} - \eta\sin(2\tau) = 0, \qquad \frac{\partial\eta}{\partial z} + \frac{\partial\zeta}{\partial\tau} = \frac{h}{2\pi}\frac{\mathrm{d}}{\mathrm{d}z}\int_0^{2\pi}\eta\,\mathrm{d}\tau, \tag{E.9}$$

where c and h is as defined in (2.5) and (2.6). In the $\sigma_0 = \infty$ limit and with the symmetry of the pressure forcing, these equations simplify to

$$\xi + \frac{\partial\eta}{\partial\tau} = 0, \qquad \frac{\partial\zeta}{\partial\tau} + \frac{\partial\eta}{\partial z} = 0, \tag{E.10}$$

from which we obtain

$$\xi(\tau, z) = -\frac{\ell}{(4m^2-1)^2}\left[1 - \frac{\cosh\left(k(z-\frac{1}{2}\ell)\right)}{\cosh\left(\frac{1}{2}k\ell\right)}\right]\cos(2m\tau), \tag{E.11}$$

$$\zeta(\tau, z) = -\frac{k\ell}{4m^2(4m^2-1)^2}\left[\frac{\sinh(k(z-\frac{1}{2})\ell)}{\cosh(\frac{1}{2}k\ell)}\right]\cos(2m\tau). \tag{E.12}$$

We now match these solutions to the Ia outer shear layer of §4 and Appendix B. In the circular limit, we have $\bar{B} = -1$, and $h = 1$. The operator (B.2) for the shear-layer eigenfunctions then simplifies to

$\mathscr{L}(Y) \equiv -Y'''' - Y''$. The eigenfunctions and eigenvalues are then given by

$$Y_n(\tau) = \frac{1}{\sqrt{\pi}} \cos(2n\tau), \qquad \mu_n = 2n(4n^2 + 1)^{1/2}, \tag{E.13}$$

where we have applied the normalisation (B.3). Now, comparing the bulk solution (E.7) and (E.11)–(E.12) as $z \to 0$ with the Ia shear layer solution (B.7)–(B.9) as $\check{z} \to \infty$, and noting that $\check{D}_n = \check{E}_n = 0$ from (7.32), we find that

$$\check{B}_n = 0 \quad \text{for} \quad n \neq m, \qquad \check{B}_m = \frac{3\sqrt{\pi}(1-\nu^2)k\ell\mu_m}{m^2(4m^2-1)^2} \tanh\left(\tfrac{1}{2}k\ell\right). \tag{E.14}$$

This result for the $\check{B}_n$, together with the expression (E.13) for the eigenfunctions $Y_n(\tau)$ and eigenvalues μ_n can be substituted into the matched solutions in §7.4. The results are compared with the full solutions in §10.

F. Regime Ib asymptotic bulk shear-layer solution in the circular limit

The aim of this appendix is to compute the axial functions $q_n(\hat{z})$ for an axially uniform pressure forcing of $\tilde{p} = -\cos(2m\tau)$ for $m \in \mathbb{Z}^+$ in the limit of a circular cross-section. The $q_n(\hat{z})$ are the solutions to (8.20)–(8.21), with the Q_n given by (C.8).

In the circular limit, the eigenfunctions and eigenvalues are again given by (E.13). From (C.8), we have that

$$Q_n = -\int_0^{2\pi} \frac{\partial^2 \tilde{p}}{\partial \tau^2} Y_n(\tau)\, d\tau = -\frac{4m^2}{\sqrt{\pi}} \int_0^{2\pi} \cos(2m\tau) \cos(2n\tau)\, d\tau = -4m^2 \sqrt{\pi}\, \delta_{nm}, \tag{F.1}$$

where δ_{nm} is the Kronecker delta.

Since the Q_n are uniform in $\hat{z}$, the solution to (8.20)–(8.21) for q_n can be written as

$$q_n(\hat{z}) = -\frac{Q_n}{2k_n^2} \left\{ \hat{z}(1-\hat{z}) + \frac{\cosh k_n(\hat{z} - \tfrac{1}{2}) - \cosh(\tfrac{1}{2}k_n)}{k_n \sinh(\tfrac{1}{2}k_n)} \right\}, \tag{F.2}$$

where $k_n = \ell \tilde{\mathscr{F}}^{1/2} \mu_n$.

In Regime Ib, we have $\tilde{\mathscr{F}}^{1/2}\ell \ll 1$. Provided n is not too large, we will have $k_n \ll 1$. We can then use the Taylor expansions of the hyperbolic functions in (F.2) to obtain the simpler asymptotic expression

$$q_n(\hat{z}) \sim -\frac{1}{24} Q_n \hat{z}^2 (1-\hat{z})^2. \tag{F.3}$$

Hence for the pressure forcing $\tilde{p} = -\cos(2\tau)$ we have, at leading order,

$$q_1(\hat{z}) = \frac{\sqrt{\pi}}{6} \hat{z}^2 (1-\hat{z})^2, \qquad q_n(\hat{z}) = 0 \quad \text{for } n \geq 2. \tag{F.4}$$

This result for the $q_n(\hat{z})$, together with the expression (E.13) above for the eigenfunctions $Y_n(\tau)$ can be substituted into the matched solutions in §8.3. The results are compared with the full solutions in §10.

Acknowledgements

REFERENCES

BERTRAM, C. D. 2008 Flow-induced oscillation of collapsed tubes and airway structures. *Resp. Physiol. Neurobiol.* **163** (1-3), 256–265.

BERTRAM, C. D. & TSCHERRY, J. 2006 The onset of flow-rate limitation and flow-induced oscillations in collapsible tubes. *J. Fluids Struct.* **22**, 1029–1045.

FLAHERTY, J. E., KELLER, J. & RUBINOW, S. I. 1972 Post-buckling behaviour of elastic tubes and rings with opposite sides in contact. *SIAM J. Appl. Math.* **23**, 446–455.

FLÜGGE, W. 1972 *Tensor Analysis and Continuum Mechanics*. Springer-Verlag.

GROTBERG, J. B. & JENSEN, O. E. 2004 Biofluid mechanics in flexible tubes. *Annu. Rev. Fluid Mech.* **36**, 121–147.

HEIL, M. & HAZEL, A. L. 2011 Fluid–structure interaction in internal physiological flows. *Annu. Rev. Fluid Mech.* **43**, 141–162.

HEIL, M. & JENSEN, O. E. 2003 Flows in deformable tubes and channels: Theoretical models and biological applications. In *Flow Past Highly Compliant Boundaries and in Collapsible Tubes* (ed. P. W. Carpenter & T. J. Pedley), chap. 2, pp. 15–49. Kluwer Academic, Dordrecht.

KECECIOGLU, I., MCCLURKEN, M. E., KAMM, R. D. & SHAPIRO, A. H. 1981 Steady, supercritical flow in collapsible tubes. Part 1. Experimental observations. *J. Fluid Mech.* **109**, 367–389.

MCCLURKEN, M. E., KECECIOGLU, I., KAMM, R. D. & SHAPIRO, A. H. 1981 Steady, supercritical flow in collapsible tubes. Part 2. Theoretical studies. *J. Fluid Mech.* **109**, 391–415.

NETHERWOOD, D. J. & WHITTAKER, R. J. 2023 A new solution for the deformations of an initially elliptical elastic-walled tube. *Q. J. Mech. Appl. Math.* **76** (1), 49–77.

SHAPIRO, A. H. 1977 Steady flow in collapsible tubes. *ASME J. Biomech. Engr* **99**, 126–147.

WALTERS, M. C. 2016 *The Effects of Wall Inertia and Axial Bending on Instabilities in Flow through and Elastic-Walled Tube*. PhD Thesis, University of East Anglia. Available online at https://ueaeprints.uea.ac.uk/58536/.

WHITTAKER, R. J. 2015 A shear-induced boundary layer near the pinned ends of a buckled elastic-walled tube. *IMA J. Appl. Math.* **80** (6), 1932–1967.

WHITTAKER, R. J., HEIL, M., JENSEN, O. E. & WATERS, S. L. 2010 A rational derivation of a tube law from shell theory. *Q. J. Mech. Appl. Math.* **63** (4), 465–496.

UNCORRECTED MANUSCRIPT